Sun resonant forcing of Mars, Moon, and Earth seismicity

Mensur Omerbashich

https://orcid.org/0000-0003-1823-4721, editor@geophysicsjournal.com

Global seismicity on all three solar system's bodies with *in situ* measurements — Earth, Moon, and Mars — is due mainly to Rieger resonance (RR) of the solar wind's macroscopic flapping, driven by the well-known P_{Rg}=~154-days Rieger period and detected commonly in most heliophysical data types and the interplanetary magnetic field (IMF). Thus, spectra of InSight B/C-quality marsquakes rates revealed P_{Rg} as the only 99%-significant spectral peak in the 1–6 months (385.8–64.3-nHz) band of highest planetary energies. While a very high (>>12) fidelity $\Phi=2.8\cdot10^6$ characterizes P_{Rg} at Mars, modular $1/2P_{Rg}$ and $1/3P_{Rg}$ Rieger-type periodicities are co-driving Martian seismicity, at 89%–67% significance, and Φ>>12. A longer (v.9) release of InSight raw data revealed the entire RR, excluding a tectonically active Mars. Previous marsquakes studies showed a preference for higher frequencies, localization, temporal (dusktime) clustering, and annual variation — features that, taken together, are typical of a forced resonator. For check, I analyze rates of Oct 2015–Feb 2019, M_w5.6+ earthquakes, and all the Apollo moonquakes. To decouple magnetosphere and IMF effects, I analyze Earth and Moon seismicity during traversals of the Earth magnetotail vs. IMF separately. As shown with 99–67% confidence and Φ>>12, an unspecified majority of M_w5.6+ earthquakes and moonquakes also recur at RR periodicities, while about half of the spectral peaks split — but also into clusters that average to RR components, where magnetotail reconnecting clears the signal. The repeating of the Mars result for Earth and Moon means the solar wind co-drives geophysics, selenophysics, and areophysics. Without getting into causal mechanisms in detail, previous claims on solar wind/plasma dynamics being seismogenic are confirmed. This result calls for a reinterpretation of the seismicity phenomenon and reliance on global magnitude scales. Predictability of the solar wind threat is beneficial for physics-based seismic prediction and forecasting, and for the safety of space missions and solar system installations.

Key words— Mars; The Moon; Earth-moon system; Earth (planet); Lunar seismology; Magnetohydrodynamics; Solar wind; Plasma astrophysics; Plate tectonics; Period search.

1. Introduction

Plate tectonics is not the ultimate Earth theory (Jacoby, 2001), and classical approaches based on the heat transfer geophysical hypothesis and from it deriving mantle convection models failed to help us understand why the Earth has plate tectonics in the first place (Stevenson, 2008). From the viewpoint of fluid dynamics, for example, mantle convection is a simple phenomenon: a typical velocity of this convective flow is only a few cm/yr, while kinetic energy is comparable to the kinetic energy of a car running on a freeway, and therefore negligibly small compared with the rate of total potential energy release (Ogawa, 2007). Besides defying basic logic thus, mantle convection models also contradict crucial data known for a long time, like the uppermost mantle's very high M_w6+ velocities of over 8.5 km/s (Yegorkin and Chernyshov, 1983). In simplest terms, mantle convection models by design break down if one can demonstrate a coupling between continents and flows in the mantle — for example, a widely held model by Richter and McKenzie (1977).

To demonstrate one such continent-mantle global coupling mechanism, Omerbashich (2020a) approached the problem from the mechanical resonance perspective instead, thus successfully extracting Earth's body (mechanical) superharmonic resonance from global tectonic earthquakes occurrences. That approach resulted in the first successful extraction of the globally controlling mechanism for initiating and triggering seismic events and sequences. Ferrazzini and Aki (1987) demonstrated that mechanism previously for tremors (Gupta, 2011). This successful extension of a local seismicity mechanism to global scales indicated global resonance plate tectonics, which Omerbashich (2021a) then successfully demonstrated from continuous GPS measurements as actual waves in the solid matter and on continental scales. Finally, a separate demonstration of Moon-body resonance from global moonquakes by Omerbashich (2020b) provided data-based spatiotemporally independent proof of global resonance tectonics and its universal (astrophysical) character, confirming an earlier theoretical demonstration by Omerbashich (2006a) that extended this *georesonation* concept by successfully relating gravity with the speed of light on quantum and macroscopic scales. That mechanical resonance tectonics is astrophysical in character is supported by globally present km-scale Faraday latticing observed in recent years on numerous bodies in the solar system — notably abundantly on Ceres and in the form of polygonal morphology, mostly hexagonal (Omerbashich, 2020b.).

The mechanical resonance of a body is a physical phenomenon that occurs when the body's eigenperiod of vibration coincides with ("resonates to") another physical system's eigenperiod or its fractional multiple, resulting in an additional vibration ("resonance"). The nature of a matched period, i.e., whether subharmonic or superharmonic, governs the resonance. Solids exposed to a resonance tend to crumble in a structural failure. Body resonances also arise via magnified (planetary) vibration due to frequency demultiplication as one of the rarest macroscopic physical phenomena and one that can magnify the energy injected at the fundamental disturbing frequency by 100s of times (Den Hartog, 1985; Omerbashich, 2007a). As a deterministic process, resonance makes resonance seismotectonics a deterministic process also. This relation forbids stochastic processes such as the mantle convection from playing a dynamically significant role on the global level. Namely, plate tectonics is not an autonomous activity — and has continued for billions of years on the Earth with the help of some agents that break the lithosphere from the outside, resulting in continental collisions and hot mantle plumes — where continental collision is a stochastic process, while plate behavior is expected to be rather stochastic as well (Ogawa, 2007). Stochastic dynamic processes cannot drive a deterministic dynamic process; only the reverse is physically plausible. Thus the present study attempts to detect such external agents of resonance tectonics in the solar system, using *in situ* seismicity measurements from all solid bodies available: Mars, Moon, and Earth.

Most promising candidates for the external geodynamics agents presumably are located in the body's immediate vicinity, mainly the interplanetary magnetic field (IMF) carried around the heliosphere by the solar wind, whose own dynamic is locally transient. The solar system often exhibits different periodicities in electromagnetic radiation and energetic particle events, ranging from the ~11-year sunspot cycle to the 27-day rotational period (Chowdhury et al., 2008; Chowdhury et al., 2016), including various mid-range periods (Bai, 2003). During solar cycle 21, Rieger et al. (1984) found the dominant (longest) such quasi-period, P_{Rg} = ~154 days, in 139 γ-ray and >500 soft X-ray flares recorded by the Gamma-Ray Spectrometer aboard the Solar Maximum Mission. Since then, P_{Rg} has been detected in the interplanetary magnetic field in the Earth's vicinity (Cane et al., 1998) and virtually all heliophysical data sets such as various types of flares, photospheric magnetic flux, and group sunspot numbers. Those studies also reported P_{Rg}-related mid-term periodicities of ~128, ~102, ~78, and ~51 days, referred to as Rieger-type periodicities (Dimitropoulou et al., 2008), which arise as modulations of P_{Rg}: 5/6 P_{Rg}, 2/3 P_{Rg}, 1/2 P_{Rg}, and 1/3 P_{Rg}, respectively. Various longer periodicities and their modulations were reported as well — in almost all heliophysics data types. These include sunspot numbers, solar flare index, solar radio flux, proton speed, and others, except for the coronal index and 10.7 cm solar flux (Forgács-Dajka and Borkovits, 2007). While the well-known (Chowdhury et al., 2009) P_{Rg} thus can be regarded as the most obvious candidate for the external agent for shaping surfaces of terrestrial bodies, Simpson (1968) previously postulated that IMF variations could cause seismic fracturing through surging crustal currents or magnetohydrodynamic (Alfvén, 1942) coupling.

Rieger period likely originates in the Sun and is the guiding period of the solar wind in highest planetary energies, resulting in its power and thus macroscopic prominence. The process responsible for IMF disturbance at the Rieger-type periodicities primarily reflects the flapping of solar wind, plasma, and other kinds of mechanical waves (mostly made up of electrons) as they are pushed outwards by coronal mass ejections. As with any mechanical resonance that occurs when waves hit insurmountable obstacles, the Rieger-type periodicities likely are naturally occurring resonance harmonics of the electromagnetic blanket's macroscopic dynamics. In addition to reflecting the Sun resonances that are mainly rotationally induced (Singh and Badruddin, 2019), the resonance in the solar wind also arises because of the IMF experiencing various influences, as exerted by the bodies of the solar system and their own dynamics and gravitation, including excessive emissions of free electrons when affected by the solar mass ejections of protons.

In addition to its detection in the IMF, the *Rieger resonance* (RR) — comprising the Rieger period P_{Rg} and Rieger-type periodicities — is present in most types of heliophysics data in solar cycles 19–24, such as the above-mentioned flares, photospheric magnetic flux, group sunspot numbers, and proton speed. In the past, the Rieger period and Rieger-type periodicities have been reported in different ranges depending on the data, location, epoch, and methodology, as 155–160 days, 160–165 days, 175–188 days, and 180–190 days; see, e.g., Gurgenashvili et al. (2017). Most of these studies indicate a leading (longest) periodicity

ranging from 152- to 158-days, which seems to be particularly dominant in the time phase from ~1979 to 1983, corresponding to the solar activity maximum. (Chowdhury et al., 2008) The same agents that force solar activity could at least be responsible for some geomagnetic and seismic activity (Odintsov et al., 2006).

2. Methodology and data

2.1. Methodology

To analyze the seismicity occurrences, I apply the rigorous Gauss–Vaníček method of spectral analysis (GVSA) by Vaníček (1969, 1971) and compute spectra by a least-squares fit of data periodicity and trigonometric functions. The GV (Gauss–Vaníček) spectra, s_j, all had a spectral resolution of k = 1000 spectral points (frequencies) throughout, as:

$$s_j^{GVSA}\left(T_j, M_j^{GVSA}\right);\ j \in \aleph,\ j = 1 \ldots k \ \wedge \ k \in \aleph\,. \tag{1}$$

Subsequently, the method got simplified into non-rigorous (strictly non-least-squares) formats like the Lomb-Scargle technique created to lower computational burden, but which is no longer an issue. GVSA provides absolute (to data resolution) accuracy in extracting periodicities from any natural datasets (Omerbashich, 2021a). Fed raw data, i.e., analyzing data without preprocessing — including gaps padding with zeros, filtering, windowing, and tapering — the GVSA outputs spectral peaks against linear background noise levels. This kind of processing enables relative spectral computations, whose results for physical systems are directly energy-stratified, allowing for the direct separation of resonance forcers from corresponding harmonics and other systematic signal contents. Here input data are utilized in their raw form, without post-processing performed that some use to enhance spectra.

GVSA is strict in that, besides estimating a uniform spectrum-wide statistical significance in var% for the desired level, say 95%, in a spectrum from a time series with m data values and q known constituents as $1–0.95^{2/(m–q–2)}$ (Steeves, 1981) (Wells et al., 1985), it also imposes an additional constraint for determining the validity of each significant peak individually — the fidelity or realism, Φ. In advanced statistics, fidelity is a general information measure based on the coordinate-independent cumulative distribution and critical yet previously neglected symmetry considerations (Kinkhabwala, 2013). In communications theory, fidelity measures how undesirable it is (according to some fidelity criterion we devise) to receive one information when another information is transmitted (Shannon, 1948). In GVSA, fidelity thus is defined in terms of the theory of spectral analysis as a measure of how undesirable it is for two frequencies to "coincide" (occupy the same frequency space of a sample). A value of GVSA fidelity then is obtained as that time interval (in units of the timescale of the time series analyzed) by which the period of a significant spectral peak must be elongated or shortened to be π-phase-shiftable within the length of that time series. As such, Φ is a measure of the unresolvedness between two consecutive significant spectral peaks (those that cannot be π-phase-shifted). When periods of such spectral peaks differ by more than the fidelity value of the former, those peaks are resolvable. As the *degree of a spectral peak's dependence or tendency to cluster*, this criterion reveals whether a spectral peak can share a systematic nature with another spectral peak, e.g., be part of a batch or an underlying dynamical process like resonance or reflection. The spectral peaks that meet this criterion are in the LSSA software output listed amongst insignificant, and the rest amongst significant (hereafter: *physically-statistically significant peaks* or just (fully) *significant peaks* for short).

GVSA comes with a complete statistical package, in which statistical testing, significance, and fidelity estimates are all performed in parallel with the computation of spectra and refer to variance as the most natural descriptor of noise in a physical system. Thus the spectral magnitude of a peak in a variance spectrum represents the contribution of that specific frequency to the data variance, expressed in var% (percentage variance). In addition to var%, GVSA computes spectra in dB (Pagiatakis, 1999).

The spectral contents beyond the long end of the band of interest fall in the intermediate or mid-term band (Forgacs-Dajka and Borkovits, 2007) and so were of no interest here. Namely, numerous studies over the past three decades have identified and confirmed the Rieger period as a genuine driver of (Rieger-type) periodicities or harmonics in the same band, so spectral periods longer than 180 days are possibly reflections or harmonics of lower drivers still. On the other hand, spectral contents shorter than 30 days are most likely related to the Sun's rotational period as the driver, of ~27 days in duration.

2.2. Mars data

Seismic data collected in situ reveal fundamental physical properties of a heavenly body. After the Viking 2 in 1976 did not succeed in placing its seismometer on the ground (Lorenz et al., 2017), the second attempt to learn significantly about the main physical characteristics of Mars came about with the InSight mission (Interior Exploration using Seismic Investigations, Geodesy and Heat Transport) that landed in late 2018. Preliminary analyses of 2019-2020 InSight seismic data elucidated that bulk of events recorded are of high-frequency energy, are distributed spatially unevenly, and occur unusually far from the lander. At the same time, unlike earthquakes, the event rate fluctuates annually. In addition, marsquakes are a highly localized phenomenon, while only a few show discernable seismic phase arrivals. All such marsquakes occur 1,800 km from the lander, on the sunken Cerberus Fossae Plateau, one of the youngest geological structures on Mars, possibly caused by subsidence or extensional faulting. Marsquakes themselves are fundamentally different from earthquakes in several ways: for example, they are considerably smaller by seismic energy released, the strongest being the event recorded at teleseismic distances with a magnitude of ~ 3.6. Both local and seismic background noise on Mars can be significantly lower than on Earth, without the constant tremors induced by mechanical resonances. (Ceylan et al., 2021a; Ceylan et al., 2021b; van Driel et al., 2021)

Many candidate causes of Mars seismicity were looked into in the past, such as tidal force, fault activity, atmospheric coupling, landslide, and meteoroid impact; see, e.g., Knapmeyer et al. (2021), who favor the Sun declinations as the regime under which most marsquakes occur, i.e., between dusk and midnight. As interplanetary magnetism drastically increases at dusk (Walsh et al., 2014), in what follows, I use the InSight seismic data to spectrally probe the 30–180-days band of highest areophysical energies to determine if external forcing contributes to the peculiarities of Martian seismicity. The working assumption here is that a periodic signature of such forcing could expose the process itself. Because such a process excludes plate tectonics, here the physical hypothesis is that Mars has no active tectonics and thus no continuous seismicity, which is tested by spectrally analyzing occurrences of continuous (high-frequency) marsquakes detected with InSight as they make up more than 80% of marsquakes and are therefore the best temporal representative of Martian seismicity. The 30–180 band is also the range of RR — the dominant periodic forcing in the solar wind that carries the IMF; see, e.g., Russell (2001).

To investigate possible external drivers of Martian planetary dynamics, I first spectrally analyze 26 March 2019–28 March 2020 marsquakes occurrences from the Marsquakes Catalog by Clinton et al. (2021). The time interval spanned across one solar minimum. As cataloged for the 2019-2020 time interval, the InSight data reveal the planetary dynamics of Mars, which primarily is characterized by temporal clustering in the rupturing process and an orbital (with external forcing tacitly assumed as Mars samples such forcing orbitally) variation in the event frequency, Fig. 1 and Table 1. The highly localized spatial clustering of the events, and their tendency to cluster in time, indicate an external planetary forcing with a lock to a dominant forcer active during the sampling.

Also used in this study are the InSight raw seismic data release v.9 of 1 April 2022 (see statements on data), containing 1755 mixed-quality events spanning 13 Jan 2019–30 Sep 2021.

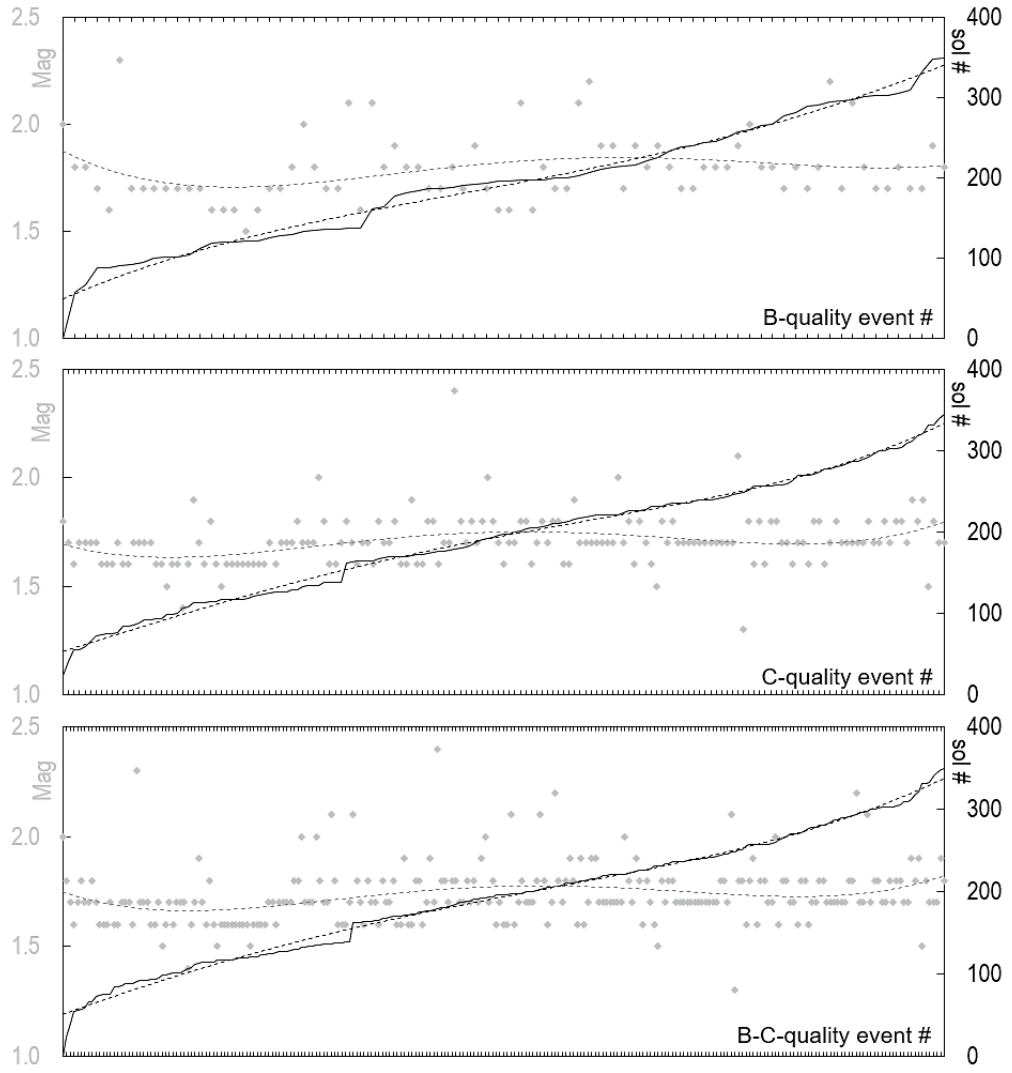

Figure 1. Marsquakes in seismic magnitudes (gray rhombs) vs. times of occurrence (solid black lines). A comparison of 78 B-quality (top panel), 163 C-quality (mid), and 241 B–C-combined-quality events (bottom) suggests that the InSight record consistently maintains the rate of events and associated trends regardless of the data quality. This conclusion is supported by 4th-order polynomial trends (dashed lines), indicating an orbitally induced variation in the event rate. The data were high-frequency events from Supplementary Table 2 of Clinton et al. (2021). Note that D-quality events were omitted here as only weakly observed or strongly contaminated by noise (Clinton et al., 2021). The data were plotted indiscriminately for a more natural depiction of driving processes. Usually, time series get depicted along artificially equipaced (presumably uniformly paced) time axes, but such representation masks nonlinear background dynamics that can only reveal themselves on their natural timescales as the only ones useful for visual inspection (remaining very involved for mathematical modeling, including linearization). The opposite applies too, and thus nonlinear timescales like the one depicted here cannot reveal equipaced variations like seasonality that cannot then be readily seen in Fig. 1, even if present in the record as claimed by Knapmeyer et al. (2021). The spectral analyses in the present study did not confirm seasonality either. However, it is possible to misinterpret portions of RR taken out of the context as a seasonality. The data shown are given in Table 1 in an analysis-ready format, with times reduced to 0-origin. Note that the spectral computations in the present study refer to the Coordinated Universal Time (UTC), but the same data in Local Mean Solar Time (LMST) produce identical results.

T(s)	Mag.	T(s)	Mag.	T(s)	Mag.	T(s)	Mag.	T(s)	Mag.	T(s)	Mag.
0	2.0	10132068	1.6	14491858	1.6	17509753	1.6	20698692	1.7	24610254	1.7
2050374	1.8	10308278	1.5	14494136	1.8	17511843	1.7	20704022	1.8	24801334	1.8
3572810	1.7	10310875	1.6	14501012	1.7	17518967	1.8	20870526	1.8	24870502	1.8
4812338	1.6	10312163	1.6	14572869	1.7	17675603	1.7	20874880	1.7	24972553	1.7
4904288	1.7	10316335	1.6	14580402	1.6	17683420	1.7	20877211	1.7	25155245	1.7
5075450	1.8	10321957	1.6	14763037	1.8	17692020	1.7	20880027	1.7	25410899	1.7
5161947	1.7	10485517	1.6	14848567	1.7	17866968	1.8	21066749	1.7	25426471	1.7
5779227	1.7	10494966	1.6	14966838	1.7	17967797	2.1	21142775	1.7	25603268	1.7
5878271	1.8	10584241	1.6	15012806	1.8	18047870	1.8	21146374	1.7	25665939	1.7
6413098	1.7	10585270	1.6	15018582	1.6	18117072	1.6	21153727	1.7	25755404	1.8
6500182	1.6	10669504	1.5	15023559	1.6	18216427	1.7	21233348	1.7	25854575	1.8
6582386	1.6	10671291	1.6	15132978	1.9	18299921	2.2	21236859	1.7	26035050	2.2
6588730	1.6	10683600	1.6	15195263	1.6	18301772	1.8	21331924	1.7	26214695	1.7
6680268	1.7	10842664	1.6	15284658	1.6	18401523	1.7	21406808	1.7	26219052	1.7
7409355	1.6	10927313	1.6	15312201	1.8	18583132	1.8	21491158	1.7	26293840	2.1
7422934	1.6	11014791	1.7	15492982	1.8	18585420	1.8	21596016	1.8	26574096	1.7
7506335	1.7	11024119	1.7	15545143	1.6	18654356	1.9	21679222	1.8	26579469	1.8
7738409	1.7	11112124	1.6	15635454	1.7	18737628	1.6	21775456	1.7	26737437	1.8
7777430	1.7	11197591	1.7	15649801	1.9	18836384	1.9	21947735	2.1	26748274	1.7
7827265	1.6	11206961	1.7	15757755	1.7	18840891	1.6	21970752	1.3	26751900	1.7
8018620	2.3	11298235	1.7	15830656	2.4	19020543	1.7	22198657	1.8	26758695	1.8
8088183	1.7	11387441	1.7	15985391	1.8	19101867	1.9	22217701	1.8	26824093	1.7
8095439	1.7	11457837	1.8	16006071	1.8	19102914	1.9	22654834	1.6	26914981	1.8
8098918	1.7	11460462	1.8	16091954	1.7	19181513	1.7	22731395	1.8	27015340	1.8
8271066	1.6	11734406	2.0	16255998	1.8	19374619	1.7	22735939	1.9	27355817	1.7
8273040	1.6	11741737	1.7	16267207	1.8	19458791	1.7	22741959	1.6	27361675	1.7
8358961	1.7	11821575	1.7	16519762	1.7	19542347	1.7	22748821	1.8	27558139	1.9
8708349	1.5	11827854	1.7	16524261	1.7	19545243	1.7	22820619	1.8	28174209	1.8
8715566	1.6	11919729	2.0	16608920	1.8	19548644	1.7	22825208	1.7	28435955	1.9
8809619	1.7	11928997	1.8	16616394	1.7	19555671	1.7	22926489	1.7	29319442	1.5
8890883	1.6	12000441	1.7	16883240	1.8	19574081	2.0	23000475	2	29321206	1.8
8899290	1.7	12084161	1.7	16912114	1.7	19640094	1.8	23279193	1.6	29416415	1.7
8982738	1.7	12099084	2.1	16963561	1.9	19814530	1.7	23442420	1.8	30098143	1.7
9153164	1.7	12172435	1.8	17003677	2.0	19903187	1.9	23624199	1.8	30481708	1.7
9428420	1.4	12177059	1.6	17143474	1.7	19991954	1.8	23887952	1.7	30812773	1.9
9523945	1.6	12185404	1.6	17166670	1.8	19995896	1.6	23893351	1.7	30985847	1.8
9866331	1.7	12269018	1.6	17321799	1.6	20002911	1.8	23904357	1.6		
9885475	1.9	12274371	1.7	17332121	1.7	20157020	1.7	23995679	1.8		
10044592	1.7	14307834	2.1	17335276	1.6	20438513	1.6	24247736	1.8		
10055291	1.6	14310432	1.8	17408558	1.6	20445137	1.5	24543478	1.6		
10128868	1.8	14401746	1.7	17435002	2.1	20518412	1.8	24601478	1.7		

Table 1. Mars data, Fig. 1, reduced to 0-origin. From the Marsquakes Catalog (corrected Supplementary Table 2 of Clinton et al., 2021).

2.3. Moon data

The moonquake data consisted of 13058 seismic events from the *Levent.1008* Moonquakes Catalog (Nakamura et al., 1981), last updated in 2008. The samplings were timestamped at a once-per-minute rate and spanned the time interval 1969–1977, as collected within the Apollo Program's passive seismic experiment—PSE/ALSEP (Passive Seismic Experiment/Apollo Lunar Surface Experiments Package), missions 11–16. Previously, Omerbashich (2020b) had used those data in their raw form to demonstrate the superharmonic resonance mechanism for generating lunar seismicity. Here I use the same data but remove meteoroid, rocket, Lunar Module impacts, and events with duplicate timestamps to enable the time-series monotony. The removal resulted in a dataset of 10815 genuine natural and unclassified moonquakes, Table A-1 in Supplement A, plotted on Fig. 2 indiscriminately for a most realistic depiction of any driving processes. The data interval spanned the entire Apollo mission's duration, including solar minima and maxima.

Since there is still no uniform definition of the moonquake magnitude, the lunar events were assigned generic random magnitudes as values of seismic magnitude in undeclared units and generated randomly from within a range delimited by two fixed select values [5.5, 7.5] (Omerbashich, 2020b). Namely, from the statistics point of view, magnitudes are irrelevant for the present study because the study is concerned not with a seismic investigation into rupturing processes (sources; sizes; locations) but a spectral (frequency) analysis of timings alone. Also, the main task in the present study is to find a 1-on-1 systematic correspondence between internal and external dynamics (not statistical correlation, since the present study is not statistical). Besides, spectral analyses in the present study were verified statistically, with periods tested for significance. However, seismic magnitudes are not critical when a widely reported ensemble of physical periods is detected (alone at that), such as a resonance train reported in the present study. The significance in such a case becomes immediately physical (100%) since the extracted information identifies itself as a physical process at once. A systematic physical process is always deterministic and only presumed stochastic — until and if such positive detection materializes. Thus, even random magnitudes from some physically realistic range will suffice for such extractions, as only timings are critical in such cases (Omerbashich, 2020a, 2020b).

From the physics point of view, as already mentioned, the randomness of seismic magnitudes does not affect the result in relative spectral analyses of time series when only previously widely reported physical periodicities are found (Omerbashich, 2020b). It is the train as a whole that is at least 67%-significant by the sheer fact that it got retrieved in its entirety. This approach is the best we can do when we lack magnitudes on a uniform seismic scale, as in the Moon case. In other words, if the body already does not act as an integrated physical system (as the minimum condition for any such detection to be statistically 67%-significant at least), no resonance train could be sustained on the global scale either. This situation results in the computed statistical fidelity values exceeding the >12 thresholds (for them to be considered reflective of a physical process; Omerbashich, 2006b, 2007b) and by many magnitudes of order, Fig. 3.

2.4. Earth data

The data represented the strong terrestrial seismicity sampled at a 1Hz rate, in moment magnitudes M_w as the most realistic (physics-based) depiction of seismicity (Kanamori, 1977) (Dziewonski et al., 1981). The data set consisted of occurrence times of all $q = 866$; $q \in \aleph$, earthquakes of $M_w5.6+$, spanning $\Delta t = 1211$ days from 01 October 2015–02 February 2019. This time-interval is chosen for its recency and completeness and because outside solar maxima or minima so that the earthquake data also serve to investigate possible effects of solar activity independently of the moonquake data that spanned both maxima and minima and of marsquake data that spanned one minimum, thus making the analysis methodologically overall most rigorous (diverse) possible. Here the time-interval should suffice for the 1–6-month band of interest; see Supplement B. The robust (outliers M** discarded) mean values from the USGS (United States Geological Survey), EMSC (European-Mediterranean Seismological Centre), and GFZ (German Research Centre for Geosciences) moment magnitudes are analyzed spectrally as:

$$\overline{M_i}|_{i=1}^{q} = \frac{1}{3}\left[M_i^{USGS} + M_i^{EMSC} + M_i^{GFZ}\right];\ \ i \in \aleph\ \ \wedge\ \overline{M_i}|_{i=1}^{q} \Leftrightarrow M_i \neq M^{**}. \tag{2}$$

Here, similarly to considerations from Omerbashich (2020a), where the data are from, it is tacitly assumed that any excess events — which were temporally and spatially close to the most energetic event for a corresponding time cluster — would overrepresent this specific seismic response to the external forcing of nonlinearity (in this case by the RR process) instead of enriching its representation. Besides, here the declustering (classically: the removal of data for a better understanding of an underlying physical process) is negligible and thus spectrally insignificant when using a spectral method blind to gaps in data, like here. Therefore, I decluster the record to eliminate redundancies and consequently exclude the 21 events that had occurred within minutes of time and geographic location of another event, thereby keeping the most energetic events per time cluster, if any. This declustering resulted in 845 occurrences of M_w5.6+ events, Table B-1 in Supplement B. Previously, Omerbashich (2020a) had used the same data to demonstrate the superharmonic resonance mechanism for generating Earth seismicity. Note that the goal of declustering here is not to exclude aftershocks as understood classically but events based on their timing, as the present study (a time-series analysis) is concerned with event timing alone and neither rupturing processes nor source size. The M_w5.6 magnitude cutoff sits at twice the lower limit of the M_w6.2±5% used for the cutoff magnitude by Omerbashich (2020a), here thus expanded for higher data density while still reflecting the seismicity generation mechanism as that revealed from the same data by ibid.

The present study examines the effects of Moon-Earth magnetotail reconnecting on both moonquakes and earthquakes. Therefore, any effects of geomagnetism on earthquakes here get ignored because geomagnetic field variations in the band of interest are unknown or unreliable at best. Namely, the quality and resolution of the existing geomagnetic field observations are available as assessed in the literature for high-frequency bands only, i.e., the spectral bands of periods shorter than the semidiurnal tide or frequencies higher than 0.825 μHz. Namely, unlike in heliophysics, the range of frequencies within which RR resides largely remains unexplored in geophysics.

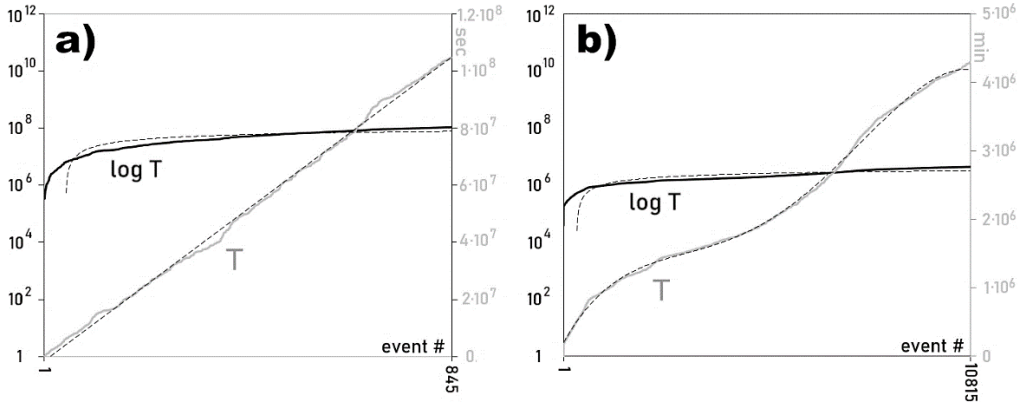

Figure 2. Occurrences, T, of 845 consecutive M_w5.6+ strong earthquakes from 2015–2019 (panel a) and 10815 consecutive natural moonquakes from 1969-1977, i.e., excluding meteoroid, S-IVB (Saturn V & Saturn IB rockets) impacts, and Lunar Module impacts, as well as events with duplicate sampling timestamp (panel b), plotted indiscriminately for a most natural representation of driving processes. Time-series data commonly are plotted along artificial equipaced (presumably uniformly paced) time axes, which, as such, mask any nonlinear background dynamics. Both panels: solid gray line represents T in seconds of Earth time (panel a) and minutes (panel b); the solid black line is the plot of log T. Also shown are corresponding trends (gray dashed): linear — revealing a nonlinear background process as it attempts to drive terrestrial seismicity but gets suppressed (panel a), and the 4th order polynomial trend — revealing a free nonlinear background process as it intensely forces lunar seismicity periodically in that process's own (unspecified) timeframe (panel b). Superimposed ideal logarithmic trends (black dashed) highlight temporal inflection points of the process. Note that the shown physical processes and trends depend on neither the event source nor rupturing size, indicating an externally induced seismicity, more so in the Moon case. Assuming IMF variations commonly generate seismicity on solid-surface bodies, the revealed trends mean the RR process affects Moon immensely and Earth to an extent. Event times reduced to 0-origin. See Supplements for data sets. Note here that the linear trend in panel (a) is for reference only, to show that a nonlinear trend exists about it, as seen from visual inspection since such relationships are too involved to be described mathematically and are beyond the scope of the present study.

2.5. Earth data and Moon data separation

Due to the inherent instability of magnetism and assuming that the RR-forced seismicity is not Mars-specific, we cannot expect the RR process to reflect on magnetospheres and the respective local IMF simultaneously. So if a planetary magnetosphere oscillates with a certain Rieger periodicity, the IMF in the vicinity of the planet does not necessarily coincide exactly with this period (or it oscillates with a different Rieger period), and vice versa.

Harada et al. (2010) used 2007–2009 data from the SELENE (SELenological and ENgineering Explorer KAGUYA) lunar mission to demonstrate the magnetic influence of the Earth's magnetic tail on the Moon. A strong electric field was detected near the lunar surface when the Moon crosses the magneto-tail, in which the plasma conditions differ significantly from those within the IMF. This relatively intensive and mutable electrical system occurs when the Moon, otherwise freed from magnetism, passes the plasma sheet, which sits centrally in the magnetic tail.

To study the effects of the geomagnetic tail on terrestrial and lunar seismicity, I make use of the mentioned blindness of the used spectral analysis method to data gaps and divide natural moonquakes into segments when the Moon was in the magnetotail (2865 events) or within three days of the Full Moon (Phillips, 2008), vs. IMF (7950 events), i.e., the remainder of the data set. The separation of the earthquake data has resulted in time series with 210 and 635 events, respectively. Indeed, this procedure revealed the zonal periodicity mismatch described above, Fig. 3. As seen from contrasting the comparisons amongst Fig. 3 a & c vs. Fig. 2 a & b, respectively, against the comparisons amongst Fig. 3 b & d vs. Fig. 2 a & b, respectively, the Earth magnetotail is indeed responsible for most of the mismatch between the lunar seismic response and RR-forcing (represented by a polynomial trend), while the process was, as expected, exposed as inherent to the IMF. Note that since this separation effect only arises when we plot the event times indiscriminately, the dataset size before vs. after the separation does not matter. The only relevant factor is a process behind the nonlinearity as revealed by this separation and in the process's own timeframe of which we know nothing, thus making any statistical analyses of the above process impossible. Besides, in spectral analyses as the core of the present study, change in dataset size due to data separation has no impact on the result (or on Figs. 2 & 3) since the used spectral analysis method is impervious to data gaps always in the same way. Thus, the relative accuracy of estimated spectra is maintained since (relative) spectral analyses are a goal of the present study.

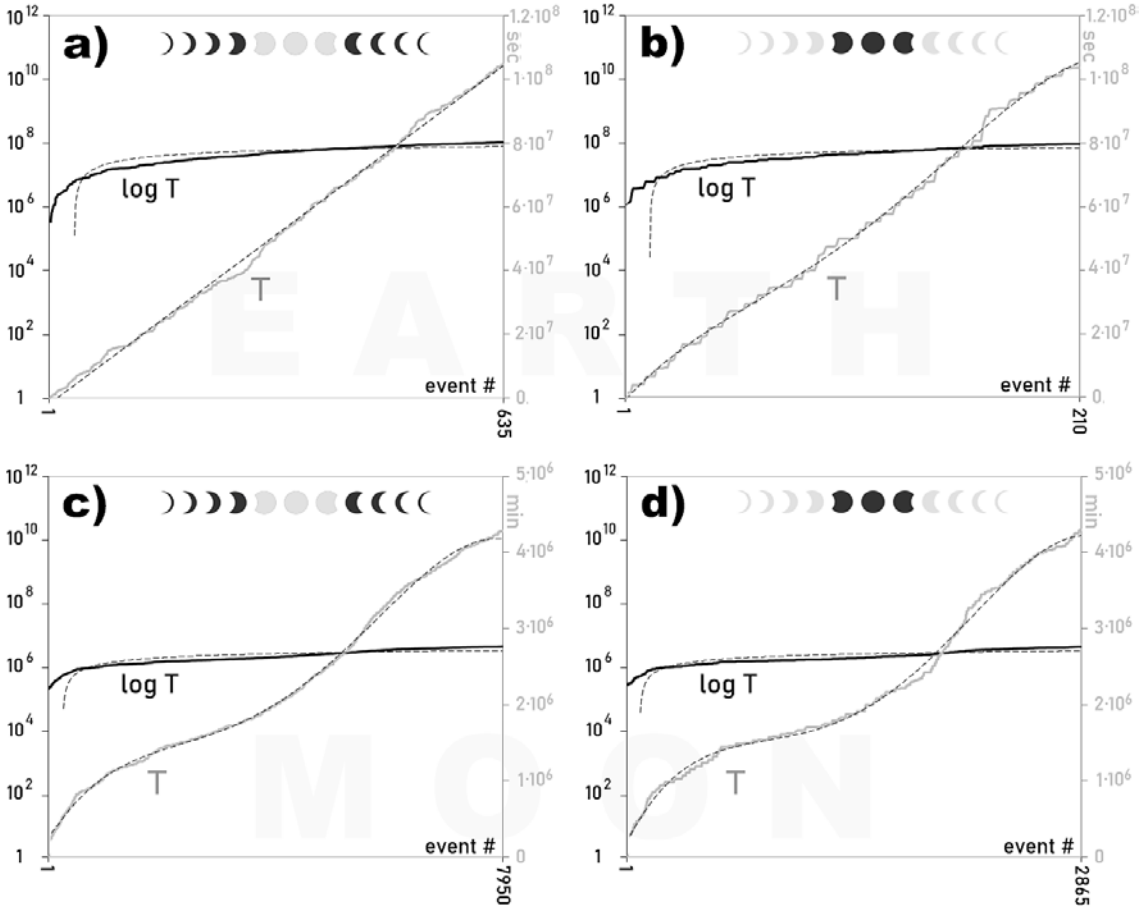

Figure 3. Indiscriminately plotted M_w5.6+ strong terrestrial (top row) and lunar (bottom) events occurrences, T, from Fig. 2, separated into events during the Moon traversals of the Earth magnetotail (panels b & d), vs. while crossing the IMF (panels a & c). As in Fig. 2, a nonlinear background driver of strong terrestrial seismicity is seen as suppressed (panel a) but then resumes nonlinearity (as fitted weakly by the 4th order polynomial) as the Moon crosses the tail. This switch from a suppressed to free nonlinearity of terrestrial seismicity occurrences when the Moon moves from the IMF to magnetotail shows that the lunar opposition disturbs a dynamic of the Earth-Moon system (body magnetism has reconnected). This dynamic is then itself seismogenic. In addition, the nonlinearity of the dominant forcing process of terrestrial seismicity is weaker than the nonlinearity of the lunar seismicity's forcing process, so different nonlinear dynamics dominate the two bodies. A significantly better correspondence of moonquakes occurrences with the 4th order polynomial in panel c vs. panel d revealed that the lunar seismicity occurrences are most faithfully nonlinear as the Moon traverses the IMF and the magnetotail affected the nonlinearity. This causality, in turn, shows that the main driver of lunar seismicity lies in the IMF, as this seismicity perhaps arises magnetohydrodynamically (Simpson, 1968; Alfvén, 1942), whereby the response of the Moon to IMF variability intensifies on each reconnection with the Earth magnetotail. Note that a magnetotail crossing here begins three days before a lunar opposition (Full Moon) and lasts for six days (Phillips, 2008), so the Moon spends about ¼ of its orbit in the Earth magnetotail. The line representation is as in Fig. 2. See Supplements for data sets.

3. Results

3.1. Mars results

Spectral analysis of the Marsquakes Catalog has revealed externally forced dynamics of Mars seismicity, Table 2 and Fig. 4. The longest periodicity detected is the widely reported Rieger period P_{Rg}=154.48 days at 4.8 var%, found to be the Mars system driver as it absorbed all power at the 99%-significance and has the highest statistical fidelity found in this study, of staggering $\phi=2.9\cdot10^6$. This detection conclusively confirms that the external forcing is dominant in Martian dynamics, as the fidelity of >12 is considered reflective of a physical process (Omerbashich, 2006b, 2007b). Other significant periods are 42.07-days at 2.5 var% with 95% significance and again very high $\phi = 2.1\cdot10^5$, then 54.51-days at 2.1 var% with 89% confidence and very high $\phi = 3.6\cdot10^5$, and 73.87-days at 1.5 var% with 67% significance and very high $\phi = 6.6\cdot10^5$.

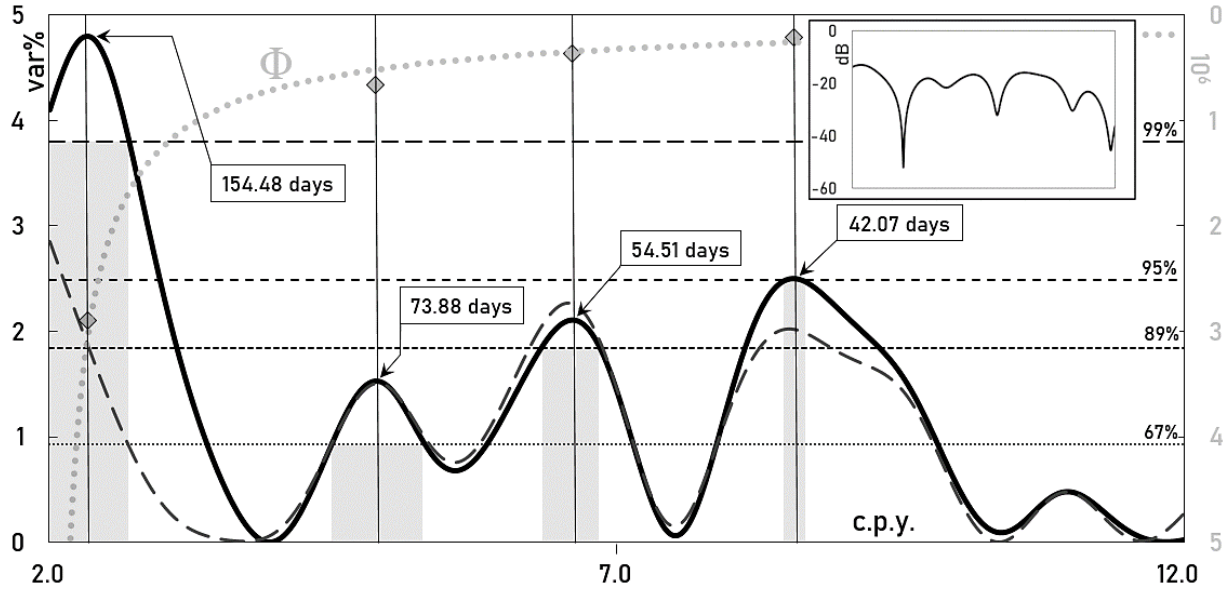

Figure 4. GV spectrum (solid curve) of data from the Marsquakes Catalog (Clinton et al., 2021) in the 1–6 months band of the highest planetary energies that exceed the environmental noise levels by magnitudes of order, so noise is methodologically filtered out and cannot be significantly implicated in the spectrum. Since a data span of twice the spectral band's lower end suffices for credible spectral analyses in that band, and the time series here spanned the selected bandwidth twice, the time-series B-C with combined quality proved sufficient for extracting the dominant forcer. Thus the Rieger period P_{Rg} = 154.48 days was returned as the system driver as it absorbed all power at the 99% level of significance, and this period has the highest statistical fidelity found in this study, of $\phi = 2.9\cdot10^6$. At the same time, the Rieger-type periodicities (harmonics) dominate the record across lower significance levels, but also with ϕ>>12, Table 2, where the fidelity of 12 and higher reflects a physical process (Omerbashich, 2006b); here ϕ-curve represents a power-trend fit of fidelity values for significant spectral peaks. Note the clustering on the $1/3\cdot P_{Rg}$ spectral peak. The spectrum in the Rieger band does not indicate any other systematic contents (including environmental seasonality, and therefore no need to model or "enforce" it further; for details see Wells et al. 1985), other than Rieger and Rieger-type periods, i.e., a resonance train. Of all high-frequency events from Clinton et al. (2021), the B- and C-quality marsquake series separately were insufficient to provide spectra with significant periodicity, so the combined B-C time series was used, as justified by the consistent maintenance of event rates, Fig. 1. The underlying spectrum (dashed curve) of the same data, but with P_{Rg} "enforced". i.e., modeled (mathematically suppressed and thus effectively removed from the spectrum during computation) (Wells et al., 1985), indicates neither additional forcing dynamics nor any areophysical systematic processes. Statistical fidelity values per spectral peak are plotted with the power trend on the secondary axis (gray axis). The area of the gray boxes represents the power absorption capacity of a spectral peak at the corresponding significance level; the local spectral span above the respective significance level determines the width of the box and, together with a variance percentage achieved by the corresponding peak, describes the absorption capacity. Callout: the power spectrum of the same data, in dB (Pagiatakis, 1999). Pronounced and broad lobes indicate that the significant spectral peaks comprise practically all the power as well. Note that non-sharp resonance peaks reflect low data resolution, as limited by scant Mars seismicity. Frequencies are in cycles per year (c.p.y.), with periods indicated on significant peaks as well. Note also that immediate outer bands shorter than the high band end belong to Sun resonance due to the rotational rate of ~27 days (Singh and Badruddin, 2019), while those longer than the low band end belong to poorly understood mid-term periodicities (Forgacs-Dajka and Borkovits, 2007). Therefore looking into the outer bands would be counterintuitive for the present study.

Period	Significance level	T [s]	T [days]	T_{solar} [days]	ΔT [%]	Φ	Mag. [var%]	Power [dB]
P_{Rg}	99% (3.80 var%)	13347464	154.485	154	–0.3	$2.9 \cdot 10^6$	4.8	-12.97
$1/2 \cdot P_{Rg}$	67% (0.93 var%)	6383093	73.878	78	+5.3	$6.6 \cdot 10^5$	1.5	-18.09
$1/3 \cdot P_{Rg}$	89% (1.84 var%)	4709442	54.507	51	–6.9	$3.6 \cdot 10^5$	2.1	-16.67
$3/11 \cdot P_{Rg}$	95% (2.49 var%)	3635107	42.073		–0.1	$2.1 \cdot 10^5$	2.5	-15.91

Table 2. Results of GV spectral analysis, Fig. 4, of the Marsquakes Catalog, Fig. 1. The previously reported P_{Rg}, $1/2 \cdot P_{Rg}$, and $1/3 \cdot P_{Rg}$ got matched, while the previously reported $5/6 \cdot P_{Rg}$ and $2/3 \cdot P_{Rg}$ periods got absorbed by P_{Rg}. Note the degeneration of the $1/3 \cdot P_{Rg}$ within the Mars vicinity into a $3/11 \cdot P_{Rg}$ split. Also, note that the above-given agreement (ΔT) with previously reported such periods T_{solar} is the upper limit (the worse) of such matchings, while $1/2 \cdot P_{Rg}$ and $1/3 \cdot P_{Rg}$ were also previously reported as in the present study, e.g., by Özgüç and Ataç (1994). The Ts_{olar} value for P_{Rg} is per Chowdhury et al. (2009), and for the $1/2 \cdot P_{Rg}$ and $1/3 \cdot P_{Rg}$ harmonics per Dimitropoulou et al. (2008).

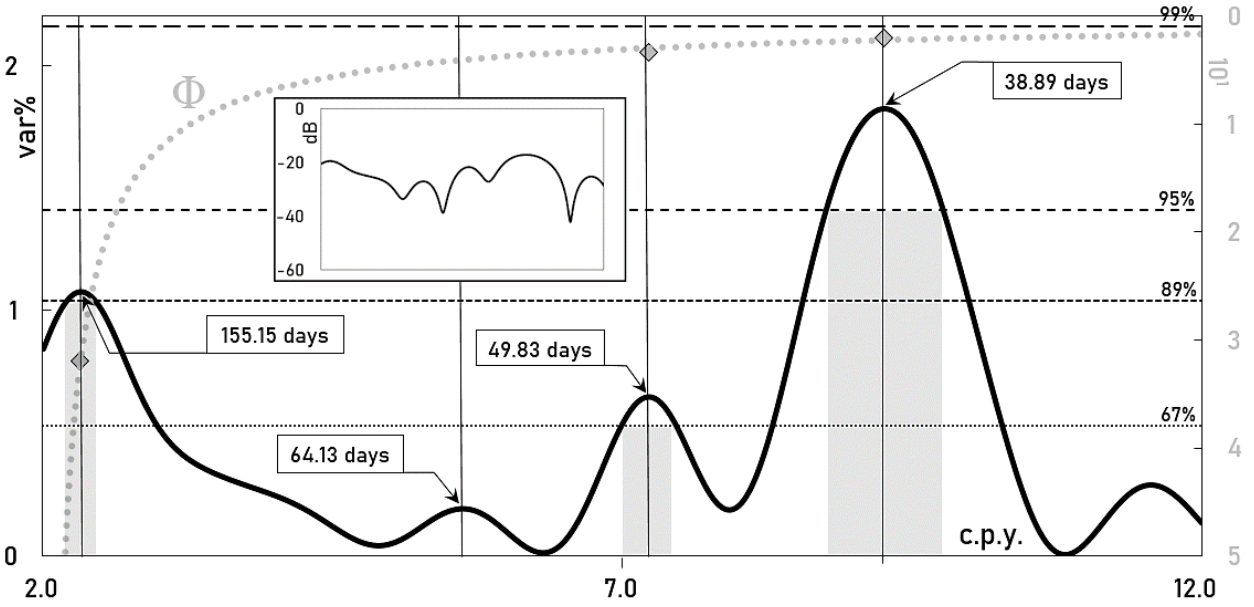

Figure 5. Same as Fig. 4, but of all 424 B–C–D-quality high-frequency marsquakes combined, thus including the 183 D-quality events with random seismic magnitudes. Periodicity estimates largely were preserved (to within a few days). Also plotted is the corresponding power spectrum (callout), revealing that the P_{Rg} driver still absorbs most power. Note that the detected resonance peaks did somewhat sharpen compared to Fig. 4, and more so on harmonics, as expected when increasing data resolution (herein by roughly doubling it).

When the record includes D-quality events, periodicity estimates get largely preserved (to within a few days), where the driver estimate remains the same (to ±1 day), Fig. 5. Significance levels went somewhat down (but not below the resonance) due to the poor quality of D events and the use of random magnitudes since D-quality marsquakes did not have any seismic magnitudes assigned to them. This overall drop in the quality is also seen from the statistical fidelity lowering by five orders of magnitude compared to the spectrum of B–C-quality events combined, Fig. 4. The above is an example of GVSA not requiring real-world variations to estimate/verify a known set of frequencies, as long as random magnitudes are constrained by some realistic range; here 1.0–2.5. In this case, a train of well-known natural resonance is extracted from a record of real-world seismic occurrences from another planet with 43% of magnitudes selected at random, where the driver estimate preserved the $\phi > 12$ fidelity threshold indicative of a physical

process. The recovered ensemble's power stayed within the 20–40 dB range that from B–C events combined (callout vs. Fig. 4 callout). The thus demonstrated ability to extract systematic information from sparse and incomplete (here missing nearly half of total variations) records of real-world data taken in situ in another world highly recommends GVSA not just to planetary seismologists but to everyone else interested in learning a whole lot about the unknown when very little information is available. Be it noted here that GVSA requires just three values to estimate a spectrum.

The above recovery of RR from the Marsquake Catalog by Clinton et al. (2021) was partial. Since this could not be due to data span, to examine if it was due to heavy editing of raw data by ibid., I next spectrally analyze the most recent/complete (at the time of writing the present study) release of InSight raw seismic data, v.9, of 1 April 2022 (see statements on data). Since the events were of varying and unknown quality while lacking seismic magnitudes on a unique scale, and given the promising analysis of events with random magnitudes, Fig. 5, I assigned seismic magnitudes randomly from within a range delimited by two fixed select values [1.0, 3.0]. This extended range appeared realistic for this (v.9) release of raw data because events increased somewhat in strength since Clinton et al. (2021) published their results. If — unlike the shorter data edited by ibid. that revealed partial RR, Figs. 4 & 5 — raw data with random seismic magnitudes expose the complete RR, then Martian seismicity likely is due to RR entirely, meaning Mars is a tectonically inactive planet. If so, then marsquakes classification by quality or another RR-unrelated criterion loses any physical meaning also.

As seen from Fig. 6, GVSA of v.9-release raw data in the 30–180 days band has indeed recovered the complete RR: P_{Rg} as 169.8-days with most of the power (callout) and Φ>12, and all of the commonly reported harmonics (Dimitropoulou et al., 2008): ~128-days as 129.5-days, ~102-days as 105.2-days, ~78-days as 79.4-days, and ~51-days as 52.2-days, Table 3. The harmonics were reported from data collected throughout the solar system and are thus not exclusive to Mars, so they are external and all more believable as the causal mechanism of marsquakes. On the other hand, the GVSA-extracted values of RR harmonics are all phase-shifted in the same sense by ~1-days from the respective commonly reported values, Table 3, thus confirming the high quality of GVSA as a method while indicating Mars-only features that affect RR harmonics in such a uniform way. The previous point is emphasized by serial anisotropic peak splitting (but to clusters that average to RR periodicities), Fig. 6. The above values are at least 67%-significant, except for the 102.5-days period that is significant at or above 63%, but this is of no concern given that the period is part of a well-known ensemble of >67%-significant harmonics.

P_{Rg} shifted from 154.5-days, Fig. 4, to 169.8-days, Fig. 6, or the previously unreported 165–175-days range (Gurgenashvili et al., 2017). This shifting was likely due to a combination of the transient nature of P_{Rg} and - since the shift occurred in the same sense as when B/C events expanded to D-quality, Fig. 5 vs. Fig. 4 - a mixed quality of v.9-release raw data as well. For a test (not shown), extending the spectral band to 1–9 months (30–270 days) resulted in the recovery of P_{Rg} at an insignificantly different value of 170.39-days at >67% significance, confirming GVSA qualities rooted in this method's features such as the unique handling of spectral leakages and the non-dependence on the Nyquist frequency.

Period	Significance level	T [days]	T_{solar} [days]	ΔT [%]	Φ	Mag. [var%]	Power [dB]
P_{Rg}	67% (0.13 var%)	169.80	154	-10.3	15.0	0.2	-27.74
$5/6 \cdot P_{Rg}$	95% (0.34 var%)	129.46	128	-1.1	8.4	0.4	-24.51
$2/3 \cdot P_{Rg}$	63% (0.11 var%)	105.22	102	-3.2	5.6	0.1	29.44
$1/2 \cdot P_{Rg}$	99% (0.52 var%)	(79.38)	78	-1.8	3.2	0.6	-22.32
$1/3 \cdot P_{Rg}$	95% (0.34 var%)	(52.19)	51	-2.3	1.7	0.4	-24.44

Table 3. Results of GV spectral analysis, Fig. 5, of the release v.9 of InSight raw seismic data of 1 April 2022. The T_{solar} common values for P_{Rg} and harmonics are as in Table 2. Averaged values from clusters of split spectral peaks are in parentheses, while other respective values refer to the majority of spectral peaks in a spectral cluster, Fig. 6.

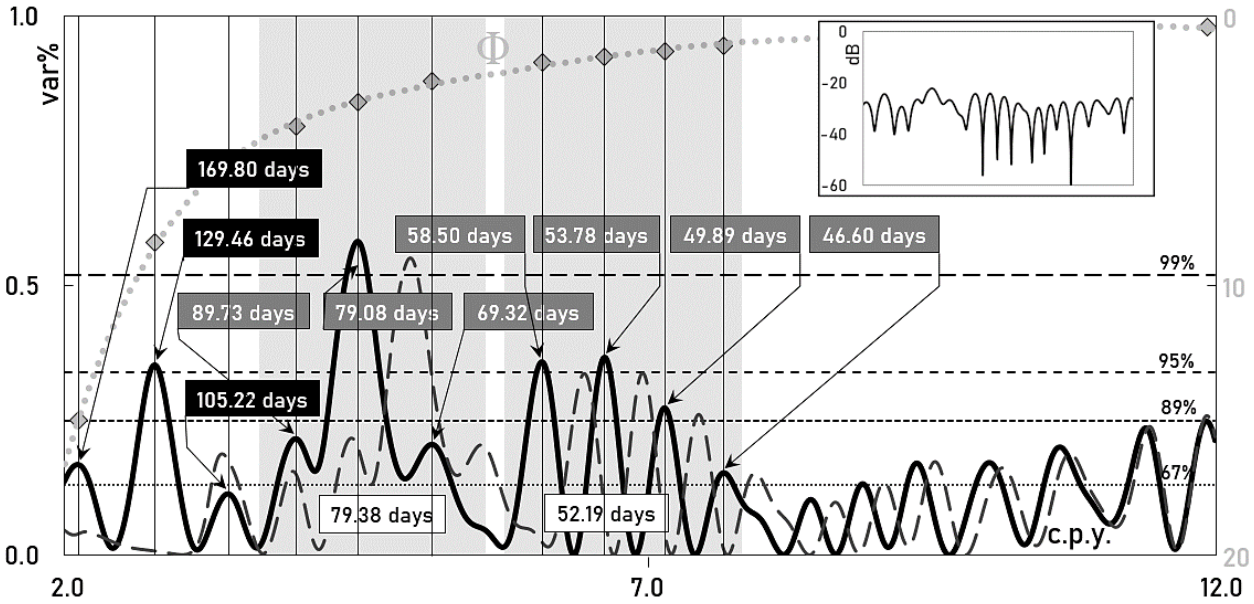

Figure 6. GV spectrum (solid curve) of all 1755 events from the 1 April 2022 release v.9 of the InSight raw seismic data in the 1–6 months band of the highest planetary energies. RR periods highlighted in black. The dashed solid curve represents the spectrum of the same data but after enforcing (mathematically removing the effects of; see, e.g., Wells et al., 1985) P_{Rg}. The enforcing has somewhat reshuffled power in spectral peaks and introduced a slight phase shift in the high-frequency end of the spectra, but the train configuration is largely preserved — as another indication that the extracted periods represent a single physical process. Gray boxes mark subbands of spectral peak clustering, with values of clustering periods highlighted in gray and cluster-averaged values in white. Callout: power spectrum of the same data.

3.2. Moon results

As found for Mars, celestial bodies sample the IMF-resident RR process rotationally. Thus, as it orbits Earth, the magnetism-stripped Moon scans the Earth magnetotail (for ~1/4 of a revolution or synchronous rotation) and the IMF (~3/4). As a result of the constant mutual interference by the smaller and intrinsic magnetism-freed Moon against the more massive and magnetically shielded Earth, half of the RR periodicities in earthquakes occurrences and five of six periodicities in moonquakes occurrences split as the Moon traverses the IMF, Fig. 7 — but into clusters that in all cases average to RR periodicities as well, same as for Mars, Fig. 6.

In addition, the connection of the Moon with the Earth magnetosphere significantly reduces the interference (clears the signal), thereby reducing the total number of split spectral peaks in the terrestrial seismic response to the RR process from 3 to 2, Fig. 7-c vs. Fig. 7-b, and in the lunar response, from 5 to 3, Fig. 7-f vs. Fig. 7-e. Note that spectral magnitudes in lunar seismicity spectra are also here, as in (Omerbashich 2020a, 2020b), an order of magnitude smaller than in terrestrial seismicity spectra, as expected since the energy emissions from moonquakes are considerably lower than from earthquakes. This energy-proportional response, sensed naturally by variance spectra, is reflected in the power spectra as narrower and less pronounced gray lobes, see left vs. right column of Fig. 7. Also, note again that a significance level of or above 67% suffices for validating physical period ensembles that get frequently reported, as is the case here.

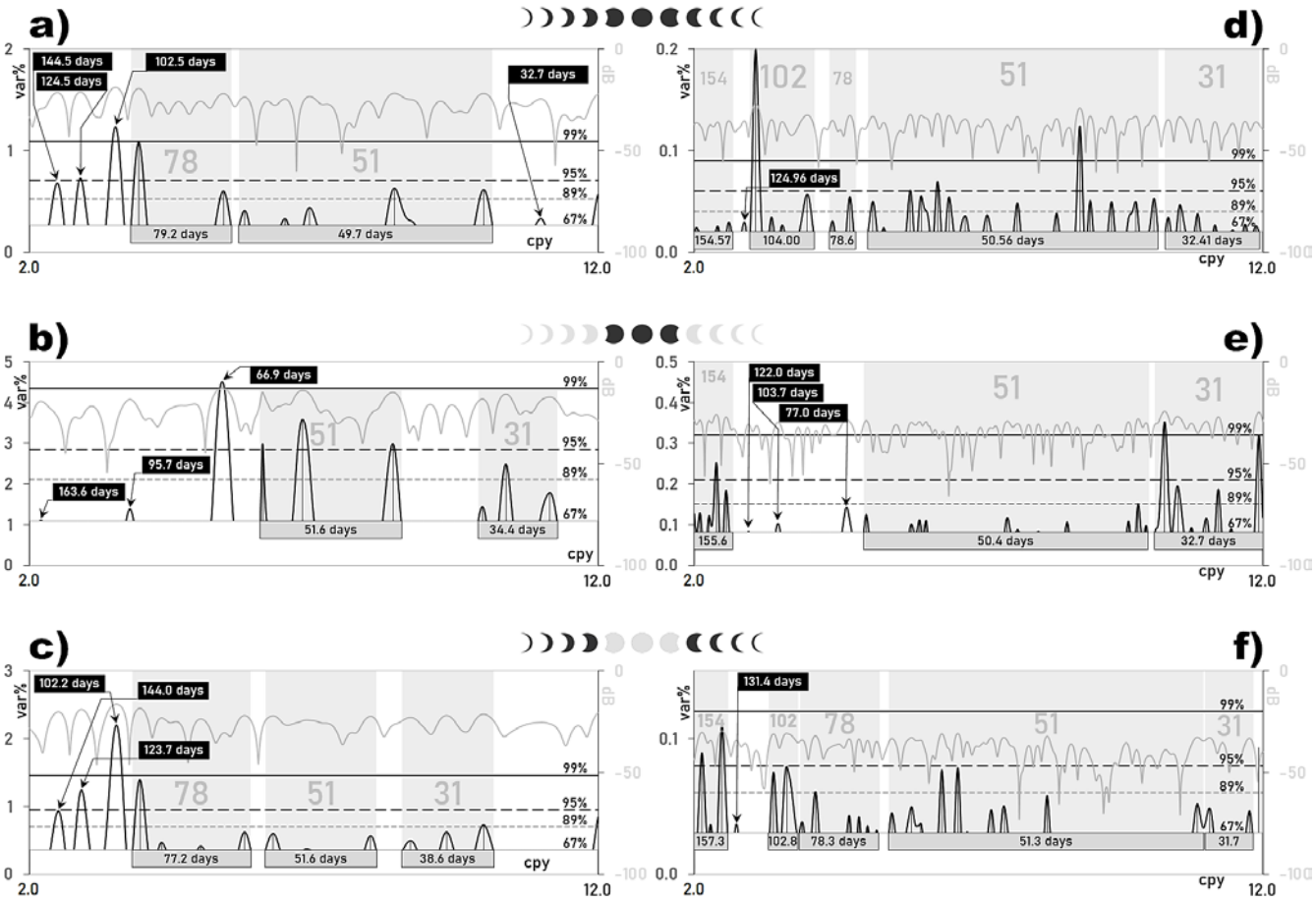

Figure 7. Significant peaks of GV variance spectra (dark line), in var%, and power spectra (gray), in dB — of terrestrial (left column) and lunar (right) seismicity occurrences, Figs 2 & 3 and Supplements A & B. Shown are spectra of all events in Supplement Tables A-1 & B-1 (top row, left-to-right), events in Tables A-2 & B-2 while the Moon was traversing Earth's magnetotail (middle), and events in Tables A-3 & B-3 while the Moon was crossing the IMF (bottom). In all cases, events responded with all RR periodicities, except when the Moon traversed the magnetotail, which led to a suppression of the 128-day primary harmonics in terrestrial seismicity (panel b). Despite the splitting into clusters (gray boxes) within relatively powerless spectral subbands (gray lobes become narrower or less pronounced), all clusters too average to RR periodicities, Table 4. Statistical fidelity for the above spectra is astounding (Φ>>12), ranging from low to high frequencies as $7.5{\cdot}10^6$–$3.8{\cdot}10^4$ and $7.5{\cdot}10^3$–$2.2{\cdot}10^2$ for terrestrial and lunar seismicity, respectively, where already Φ>12 is considered reflective of a physical process (Omerbashich, 2006b). RR periodicities reported most often are 154-, 128-, 102-, 78-, 51-, and 31-days, but, depending on data type/epoch and processing methodology, the periods were reported in other ranges as well; see, e.g., Gurgenashvili et al. (2017). Note that non-sharp resonance peaks reflect low data resolution, as limited by the scantiness of Moon seismicity and M_w5.6+ Earth seismicity. Frequencies are in cycles per year (c.p.y.), with periods indicated on significant peaks also. Frequencies in cycles per year (c.p.y.), band 30–180 days.

The non-stratified lunar seismicity shows no clear orbital preference; thus, moonquakes had occurred more frequently neither when the Moon was in the Earth magnetotail nor the IMF. The interference of RR waves by the magnetotail has increased the power both band-wide (widened or otherwise more prominent lobes in power spectra) and in GVSA-typical representations of field energy levels against the linear variance background (Omerbashich, 2007a), seen here as spectral peaks doubling in magnitudes, middle row of Fig. 7.

The difference in the spectral frequencies of global seismic responses of the Moon and Earth to the IMF-resident RR process, Fig. 8 and Table 5, measures the mismatch of individual RR periodicities due to differ-rent dynamics that influence the ecliptic-covering blanket of solar ejecta and solar wind. This mismatch can serve as a gauge for dynamically estimating the wavelengths of the RR and mapping its change with time.

The main reason prior spectral investigations into earthquakes and moonquakes occurrences returned no RR periodicities lies in analyzing events during traversals of IMF and magnetotail combined. For instance, Bulow et al. (2007) examined the time series of deep moonquakes only, which, since the present study relied on the seisms mostly, should have given similar results had those authors also separated the events in the above way. Namely, when all the events are analyzed combined, the resulting spectra encompass the RR process, albeit masked behind a combined magnetotail and magnetosphere interferences, so that moonquakes spectra return clustered periods only, Fig. 7-d. In earthquakes, such spectra cluster for most of the band, and the lowest RR frequencies get significantly mismatched due to other geodynamical drivers sharing the high-energies bands.

T [days]	T_{Rg} [days]	T'_{Rg} [days]	ΔT [days]	ΔT [%]	T [days]	T_{Rg} [days]	T'_{Rg} [days]	ΔT [days]	ΔT [%]	T [days]	T_{Rg} [days]	T'_{Rg} [days]	ΔT [days]	ΔT [%]	T [days]	T_{Rg} [days]	T'_{Rg} [days]	ΔT [days]	ΔT [%]
From 845 (total) earthquakes:					From 10815 (total) natural moonquakes:					From 2865 magnetotail natural moonquakes:					From 7950 IMF natural moonquakes:				
144.550	144.5	154	9.45	6.1%	176.467					171.420					169.004				
124.529	124.5	128	3.47	2.7%	149.352					159.274					157.875				
102.520	102.5	102	-0.52	-0.5%	137.899	154.6	154	-0.57	-0.4%	151.236					145.133	157.3	154	-3.34	-2.2%
91.792					124.962	125.0	128	3.04	2.4%	140.594	155.6	154	-1.63	-1.1%	131.351	131.4	128	-3.35	-2.6%
66.625	79.2	78	-1.21	-1.5%	116.842					121.995	122.0	128	6.01	4.7%	106.151				
62.243					107.099					103.702	103.7	102	-1.70	-1.7%	99.403	102.8	102	-0.78	-0.8%
55.432					101.651					77.044	77.0	78	0.96	1.2%	92.500				
51.986					90.407	104.0	102	-2.00	-2.0%	71.670					87.122				
42.774					81.220					64.940					76.227				
36.043	49.7	51	1.30	2.6%	76.066	78.6	78	-0.64	-0.8%	61.921					73.576				
32.730	32.7	31	-1.73	-5.6%	69.996					60.464					71.385				
					67.500					59.268					69.188	78.3	78	-0.33	-0.4%
					62.135					47.965					65.772				
From 210 magnetotail earthquakes:					60.161					46.840					61.815				
163.621	163.6	154	-9.62	-6.2%	57.377					45.709					60.161				
95.700	95.7	102	6.30	6.2%	55.517					44.687					56.654				
66.872	66.9	78	11.13	14.3%	53.217					42.073					54.261				
58.977					50.384					37.354					52.982				
52.904					46.840					36.705					49.825				
42.927	51.6	51	-0.60	-1.2%	42.978					36.188	50.4	51	0.55	1.1%	48.352				
36.116					40.971					35.025					43.869				
34.688					40.147					34.291					37.509				
32.289	34.4	31	-3.36	-10.9%	38.555					33.492					33.183	51.3	51	-0.31	-0.6%
					36.894					32.700					32.552				
					35.686	50.6	51	0.44	0.9%	32.088					31.889				
From 635 IMF earthquakes:					34.822					31.470					30.587	31.7	31	-0.68	-2.2%
143.971	144.0	154	10.03	6.5%	34.128					30.176	32.7	31	-1.75	-5.6%					
123.673	123.7	128	4.33	3.4%	33.183														
102.229	102.2	102	-0.23	-0.2%	32.260														
91.326					31.388														
83.289					30.796														
71.813					30.303	32.4	31	-1.41	-4.6%										
62.243	77.2	78	0.83	1.1%															
57.286																			
52.365																			
45.023	51.6	51	-0.56	-1.1%															
41.347																			
38.555																			
36.043	38.6	31	-7.65	-24.7%															

Table 4. Values for the GVSA spectra, Fig. 7. Listed are all significant periods, T, in terrestrial (left column) and lunar seismicity (right). Spectral peaks at RR periodicities and cluster mean values, T_{Rg}, are compared against respective most often reported values of RR periodicities, T_{Rg}'. The comparison consisted of calculating the differences, ΔT, between T_{Rg}' and T_{Rg}.

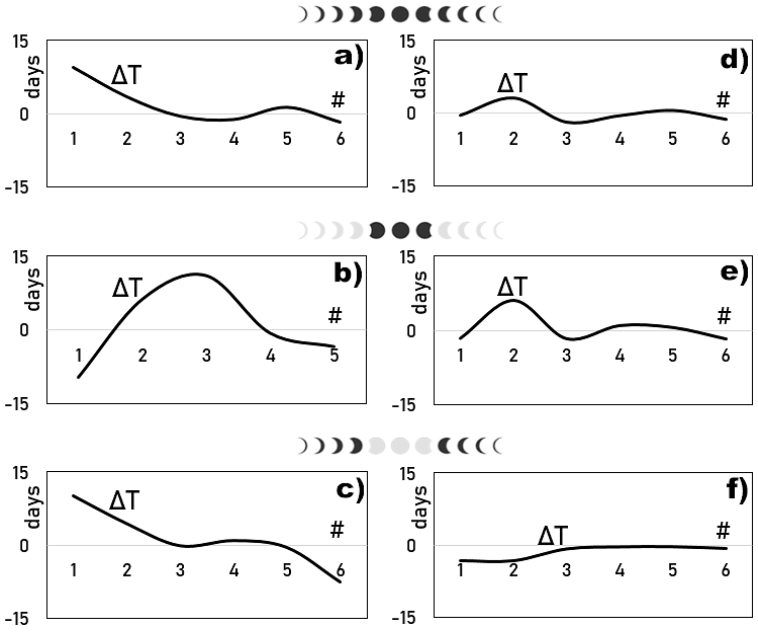

Figure 8. Matches, ΔT, of the most commonly reported RR periodicities to significant spectral peaks of earthquakes (left column) and moonquakes (right) occurrences, from Fig. 7, as differences between all GVSA-estimated significant periods from Table 1, including averages of split peaks, and the most commonly reported values of the nearest (longest six) RR periodicities, respectively: difference from ~154 days (value #1), from ~128 days (#2), from ~102 days (#3), from ~78 days (#4), from ~51 days (#5), and ~31-days (#6). Moon's passages through the geomagnetic tail cause the change in sign of the low-end mismatch as obtained from the terrestrial seismic response (to the RR process), panel b vs. panel c. Similarly, the Earth magnetotail also interferes with the lunar seismic response in lower frequencies, panel e vs. panel f. Finally, the matches for the de-magnetized Moon as it freely traverses the IMF are practically absolute across the spectral band, panel f, revealing that the IMF affects lunar seismicity more than the Earth magnetosphere could.

	P_i within tail [days]	P_i within IMF [days]	$P_i^{average}$ [days]	P_i^{common} [days]	Δ [days]	Δ [%]
Earth	163.6	144	153.8	154	0.2	0.1%
Moon	155.6	157.3	156.4	154	-2.4	-1.6%
Earth	x	123.7c	123.7	128	4.3	3.4%
Moon	122	131.4	126.7	128	1.3	1.0%
Earth	95.7	102.2	99	102	3	2.9%
Moon	103.7	102.8c	103.2	102	-1.2	-1.2%
Earth	66.9	77.2c	72.1	78	5.9	7.6%
Moon	77	78.3c	77.6	78	0.4	0.5%
Earth	51.6c	51.6c	51.6	51	-0.6	-1.2%
Moon	50.4c	51.3c	50.9	51	0.1	0.2%
Earth	34.4	38.6	36.5	31	-5.5	-17.7%
Moon	32.7	31.7	32.2	31	-1.2	-3.9%

Table 5. The match of RR periodicities as determined from the spectra of earthquakes and moonquakes occurrences, Fig. 7 and Table 4, and the most commonly reported respective values, Fig. 8. The averaged Rieger period, P_{Rg}, is closer to the most often-reported value for Earth than for Moon. All averaged Rieger-type periodicities (resonance harmonics) agree better with the respective commonly reported values for Moon than for Earth. This comprehensive inconsistency indicates that different processes dominate seismicity on the two bodies, Figs. 2 & 3. When the Moon was in the Earth magnetotail, interference suppressed the 128-days (primary harmonic), allowing the power to shift to other periods whose peak magnitudes then doubled, revealing that lunar influence on earthquakes is primarily magnetic and alternating. This suppression of a long RR period (the strongest harmonic) in the Earth's seismic response to the RR process during magnetotail-Moon reconnection shows that the Earth is only slightly better protected from the magnetically induced seismicity than the Moon is. Then the Earth's magnetosphere offers a weak shield so that even the trace magnetism of the Moon can switch off the most potent of terrestrial seismicity harmonics. On the other hand, the magnetism-free Moon responds to the entire RR process yieldingly.

3.3. Earth results

The M_w5.6+ earthquakes occurrences show the Rieger period and weak and significantly offset periods from P_{Rg}, primarily and consistently in the low-frequency (most energetic) subband of the 1–6-month band, Fig. 7-a, b, c. Such a better sensitivity of earthquakes to the RR process in higher frequencies is not only expected because the Earth is magnetically shielded but also because the lunar orbit (T_{Moon} and $1/2T_{Moon}$) coincides with the $1/5P_{Rg}$ and $1/10P_{Rg}$ resonance harmonics, respectively — so that the tidal resonance (global seismicity generation mechanism) of the Earth demonstrated by Omerbashich (2020a) comes combined with magnetic influences of the IMF and the Moon.

Hence, any geodynamical impacts of the RR process also can be understood as coincidental. Stronger (primarily gravitational-tidal) processes act on Earth resonantly (ibid.) and with frequencies that are at the same time modifications of the Rieger period. On the other hand, the Earth's magnetosphere generally appears inadequate to (entirely) filter out cosmic radiation. Thus the RR process constantly injects energy that gets resonantly magnified, contributing a significant force of geodynamics through lower parts of the atmosphere. Then this excess in irregular variability of electrons in the Earth's atmosphere is likely due to Rieger forcing of the Earth and contributes to intermittently observed variations in the total electron content (TEC). Under this scenario, the inherent instability of the magnetic shielding and the transient nature of RR help explain why the precursory qualities of TEC are rarely and irregularly, i.e., randomly, associated with earthquakes.

4. Discussion

Depending on the data, location, epoch, and methodology, RR periodicities were reported in the past in different ranges, as 155–160 days, 160–165 days, 175–188 days, and 180–190 days.; see, e.g., Gurgenashvili et al. (2017). Most of these studies indicated a leading (longest) periodicity in the 152–158-days range, which appears to be dominant, especially in the time phase from ~1979–1983, corresponding to the solar activity maximum (Chowdhury et al., 2008). The commonly reported value of this (longest) periodicity - the well-known Rieger period - is ~154 days (Chowdhury et al., 2009).

There are various proposals on the origin of the resonance process underlying the P_{Rg} period in the dynamics of Sun-ejected particles and its modulations and harmonics, including possible influences of planetary constellations on the Sun, e.g., by Kurochkin (1998) and Abreu et al. (2012). One of the few undisputed claims of this kind comes from Bai and Cliver (1990), who suggested that the P_{Rg} response could be simulated with a damped, periodically forced nonlinear oscillator exhibiting periodic and chaotic behavior. A more comprehensive explanation of P_{Rg} and its modulations is also possible, so many of the arguments put forward in the past are simultaneously justified, and the solar system harbors an interplay of resonant feedback loops amongst individual planets and the Sun. Finally, the same agents that force solar activity could be responsible for at least some geomagnetic and seismic activity (Odintsov et al., 2006).

Even though seismic magnitudes for Mars are not available on a uniform seismic scale (a situation similar to that for the Moon), they are not critical when a widely reported ensemble of physical periods is detected (and more so if detected alone), such as the resonance train reported in the present study. As mentioned, the significance in such a case becomes immediately physical (100%) since the extracted information identifies itself as a single natural process. Such processes are always deterministic — as opposed to being presumed stochastic up to the point of such positive detection. Thus, even random magnitudes from some physically realistic range will suffice for such extractions, as only timings are critical in such cases (Omerbashich, 2020a, 2020b). If the process were not deterministic, seismic magnitudes would matter when estimating the statistical significance of any periods detected. This is seen from Figs. 5 & 6 for marsquakes and Fig. 7-right for moonquakes.

The longer-spanning v.9. release of InSight raw seismic data has revealed the entire RR, Fig. 6, thus excluding a tectonically active Mars. A general view is that Mars does not have active plate tectonics

and therefore should not have continuous seismicity. The generation of InSight-sampled incessant seismicity externally (tidally-resonantly) by an electromagnetic phenomenon is supported additionally by the fact that mechanical resonance induces both small earthquakes (Ferrazzini and Aki, 1987) (Gupta, 2011) and small marsquakes (Suemoto et al., 2020; van Driel et al., 2021). Besides, both strong (M_w5.6+) earthquakes (Omerbashich, 2020a) and (mainly deep) moonquakes (Omerbashich, 2020b) can occur at tidal resonance periods. In addition, externally forced variations in the interplanetary magnetic field can lead to surges of currents in the crust, which, in turn, can trigger seismicity (Simpson, 1968). The recent MAVEN (Mars Atmosphere and Volatile Evolution) mission results by Ramstad et al. (2020) support that scenario by detecting an externally forced electromagnetism on Mars.

An alternative mechanism consists of the planetary angular velocity changes induced by a magnetohydrodynamic (MHD) coupling between the solar and planetary magnetic fields (ibid.; Alfvén, 1942). However, the lack of a magnetic field on Mars makes this scenario less likely to occur on Mars intrinsically. Therefore, external magnetic fields are required to create sustained couplings in the Mars case, such as the IMF. The Martian environment can sustain such facilitation: while Mars already possesses a weak transient magnetic field confined to very old and heavily cratered south highlands (Connerney et al., 2001), the solar wind–Mars interaction already strongly depends on the solar activity, solar zenith angle, and the altitude of interaction (Trotignon et al., 2000). When taken together, these facts greatly resemble the seismogenic environment as implied by InSight and thus support the main result of this study — on the solar wind being seismogenic.

Since Mars also reacts significantly at minima, Fig. 2 and cf. reanalysis of Viking 2 data by Lorenz et al. (2017), while the Sun only responds at maxima, Mars is closer to the source of the primary process, which then could lie in the upstream solar wind. An extensive study by Simpson (1968) supports this conclusion by showing that the frequency of non-declustered 22561 global M5.5+ earthquakes spanning 13.5 years and their weaker foreshocks and aftershocks also peaked at the solar minimum.

As indicated above, the heliophysics community itself largely remains in the dark about the time and location of the RR periodicities, just as the geophysical MHD community examines mainly subdiurnal spectral bands when investigating magnetospheric coupling, e.g., Denskat et al. (1983), instead of studying the band of highest interplanetary energies as in the present study.

Finally, the solar wind-induced seismicity on Mars, via solar wind interactions with the atmosphere, translates into a premise that day-night variations in geophysical properties of a planet are not necessarily associated with thermospheric heating (including associated wind speeds) alone. A recent report by Knapmeyer et al. (2021) supports this premise by finding that Mars seismicity is driven under the Sun declination, as the absolute majority of (high-frequency) InSight events occurred between local ~17 h and midnight. Mean current densities in the Earth magnetopause are 18 and 27 nAm^{-2} for dawn and duskside (the maximum current density in magnetotail is 10 nAm^{-2} for dawn vs. 25 nAm^{-2} for duskside), respectively. These densities are possibly due to transport via kinetic Alfvén waves during exposure to northward IMF, where the higher current density reveals the higher duskside magnetic field that also energizes faster (Walsh et al., 2014). Thus, while MHD simulations suggest that dawn-dusk asymmetry in solar wind entry by reconnection is related to ionospheric conductance (Li et al., 2008), the similarity between magnetized Earth's ionosphere and non-magnetized Mars's ionosphere (Burrell et al., 2020) makes it plausible that similar proportions of the dawn-dusk asymmetry should hold for Mars as well.

Unlike statistical correlations, which contain no physical meaning themselves and can arise purely by chance, significant peaks in the spectrum of a time series of data describing a physical system reveal the dynamics (physics) of the system. As with any mechanical resonance, which usually occurs and can even get amplified due to obstacles in its propagation paths and other reasons, the above results show that the RR process is a state of continuous mechanical resonance of the solar ejecta within the solar wind that blankets the ecliptic. The RR process gets modified as the radiation in the solar system — with the Sun as the largest emitter — encounters obstacles mainly in the form of rocky planets and moons (and probably also gaseous giants), as well as the occasional co-inclined visitor bodies such as comets that have been near the ecliptic for months or longer.

While thermal moonquakes are events caused by the day-night thermal expansion of rock at sunset, sunlight also tenuously electrifies and ionizes the Moon (Halekas et al., 2018), so a continuous magnetohydrodynamic and electrical interaction (of a weak electromagnetic field with trapped water molecules) could also be rupturing lunar rock — instead of or in combination with the thermal seismogenesis. The continuity of the interplay is supported further by a recent finding by Shang et al. (2020) that the Earth magnetotail does not constantly shield the Moon from external particles either.

Solar wind particles could also be heating the Moon's surface, as around half of the energy emitted in a solar flare is in the form of solar wind protons. The magnetic trapping of such a particle blast in the Earth magnetotail could temporarily lead to very high particle densities so that, when crossing this energized region, the surface of the Moon could become severely scorched. In addition, the IMF bound up with the solar particle blast wave could act as a magnetic bottle, retarding the dispersal of this region of high particle density on its way from the Sun. (LaViolette, 1983)

Furthermore, modeling suggests that lunar hydrogen gets cumulatively depleted as the Moon traverses the Earth's magnetotail (Tucker et al., 2021). However, the hydration part of the interplay is supported further by the recent Chandrayaan-1 mission results showing that the Earth replenishes the lunar water supply via Earth magnetotail particles during each traversal — when a particle bridge gets established between the Earth and its natural satellite (Wang et al., 2021). The Earth's magnetosphere thus has the ability needed to reconnect with lunar magnetism regardless of the weakness and instability of the latter.

Finally, the Moon's ionosphere extends when shielded by Earth, which causes the lunar plasma to measurably perturb the plasma coming from the Sun and the Earth, leading to observable variations in electrical currents and even the spatial distribution of electrons (Halekas et al., 2018).

Then, as demonstrated in the present study, the electromagnetic induction of lunar seismicity is comparable to the mechanism for inducing seismicity on Mars. However, the surging crustal currents and magnetohydrodynamic coupling mechanisms for an external generation of seismicity could influence the bodies concurrently but to a considerably different degree individually. Furthermore, since Mars and Moon feature no active plate tectonics and probably no significant tectonics of any kind, i.e., any significant strain is absent, the mechanism of seismogenesis elucidated herein is not simply a trigger mechanism. Likewise, given the absence of precipitation and large bodies of water on Mars and the Moon, lubrication is unrelated also, and this mechanism probably rests on interactions among rock-embedded water molecules and magnetically trapped plasma.

A realistic description of IMF-induced seismicity necessitates switching to advanced global seismic scales. A suitable choice is the DAS magnitude scale (Das et al., 2019; Das and Meneses, 2021), M_{wg}, which is based on global seismicity and can thus average rotational sampling of IMF-residing Rieger resonant process more faithfully than the locally tied M_w could, all while offering a better representation of Earth seismic energy budget and event emissions. As derived from already first few cycles of P-waves, the DAS global scale is fully connected to source processes and therefore is a natural descriptor of global seismogenic processes like the Rieger's. As a function of both body magnitudes, m_b, and moment magnitudes, M_o, DAS is physically refined and closely related to high- and low-frequency ground motions. Being both a subtle and global indiscriminate descriptor of seismicity, DAS is pre-tied into tectonics and recurrence processes. Its magnitudes, M_{wg}, are globally optimized, non-saturating, and provide a range-wide measure of quake size. These advantages make DAS a preferred scale of choice for planetary and lunar seismology.

Note that the here-presented statistically significant physical correspondence between internal and external lunar dynamics is more general (and therefore more plausible) than vaguely claiming that lunar seismicity is induced tidally — as often found in the literature. As mentioned above, while the RR train includes periods very close to the tidal periods (Omerbashich, 2020a) and there is no reason to exclude gravitational phenomena when considering solar-wind-induced seismicity, those two processes can couple and thus together affect selenodynamics at shared frequencies. This scenario is especially plausible given that the tidal processes concentrate stress repeatedly, and the tides pump fluids cyclically between suitably oriented shear zones (Frohlich and Nakamura, 2009), which could only aid such coupling in the driving of selenodynamics both tidally and magnetohydrodynamically.

5. Conclusions

Variance spectra of Mars, Moon, and Earth seismicity events occurrences in the highest planetary energies — which, unlike statistical correlations, measure actual system dynamics directly — are significantly periodic and only so with RR periodicities. This result, obtained spatiotemporally independently from all three bodies in the solar system for which we have in situ data, has thus confirmed (without getting into causal mechanisms in detail) previous claims that the solar wind/plasma dynamics is seismogenic due to the MHD interplay between magnetically trapped plasma and solid matter and other forms of interaction. Thus RR, as a primary underlying heliophysical process, drives areophysics, selenophysics, and geophysics, while causing the tidal-resonant fracture response that the InSight and Apollo missions and terrestrial observatories had sampled. Since the three data sets — marsquakes during a solar minimum, moonquakes during minima and maxima, and earthquakes outside either minima or maxima — refer to different and mutually non-overlapping intervals, seismicity appears to occur independently of solar activity. Therefore, locally transient undulations in the solar wind suffice for the mechanism that the present study has demonstrated beyond doubt based on all available data. For example, a noticeable degeneration of $1/3 \cdot P_{Rg}$ into a $3/11 \cdot P_{Rg}$ split peak from marsquakes, with the second-highest level of significance despite subband clustering, indicates a varying anisotropy and thus a surging interplanetary magnetic field (IMF) as felt in the vicinity of Mars. This indication and the Moon and Earth results call for landing seismic probes on other planets and moons. Such seismic missions to Europa and Titan have recently been proposed (Lorenz and Panning, 2018) and could be used to map the extent of RR in near real-time.

Since only external electro-magnetic forcing controls the band of highest energies in the Mars dynamic system and causes the only measurable continuous seismicity (as the indicator of tectonic activity), the present analysis supports the generally held view that Mars is tectonically inactive in terms of plate tectonics, thus refuting contrarian claims, e.g., recently by Banerdt et al. (2020).

The discovery of an external and principal causal mechanism of natural seismicity requires reinterpretation of the phenomenon of seismicity to encompass the physics of a body-wide fracturing response of solid matter to variations in the interplanetary and other magnetic fields. For this, advanced global seismic scales are needed, such as the DAS magnitude scale, which is globally optimized and physically balanced and can thus represent reality better while implying easy decoupling from internal (tectonic) and external (IMF's and rotational-inertial) physical processes in the Earth vicinity. Finally, based on the other two results, the Earth result could be extendable to at least some $M_w5.7$- terrestrial seismicity, while the discovered mechanism likely affects gaseous giants also.

The main result of the present study, repeated for three astronomical bodies of our solar system, provides a crude map of the planetary critical solar-wind dynamics shown here as entirely predictable. Then pending quality estimates of each RR component's wavelength, this result means that the solar wind as a threat is predictable, which will enable a higher safety of space missions and settlements and other installations on planets and moons.

Acknowledgments

I thank Dr. Ralph Lorenz (Johns Hopkins University) and Dr. Yosio Nakamura (the University of Texas at Austin) for discussions and suggestions and Barbara Pope (NASA-NSSDCA) for help with data. The least-squares spectral analysis scientific software LSSA, based on the rigorous method by Vaníček (1969, 1971), was used to compute spectra. Dr. Spiros Pagiatakis (York University) provided LSSA v.5.0, now available from http://www2.unb.ca/gge/Research/GRL/LSSA/sourceCode.html.

Declarations

The author has no competing interests or funding to declare.

Availability of data

Marsquake data underlying this article are available in Table 1 and the corrected Supplementary Table 2 of the Marsquakes Catalog at https://doi.org/10.1016/j.pepi.2020.106595, while the v.9 release of InSight raw seismic data is from the Geosciences Node of the Washington University's Planetary Data System, at https://pds-geosciences.wustl.edu/insight/urn-nasa-pds-insight_seis/data_derived/. Moonquake data are in the Supplement A, originally at https://hdl.handle.net/2152/65671. Earthquake data are in the Supplement B, originally at https://n2t.net/ark:/88439/x020219. All data used are in the public domain.

References

Abreu, J.A., Beer, J., Ferriz-Mas, A., McCracken, K.G., Steinhilber, F. (2012) Is there a planetary influence on solar activity? Astron. Astrophys. 548:A88. DOI: https://doi.org/10.1051/0004-6361/201219997

Alfvén, H. (1942) Existence of electromagnetic-hydrodynamic waves. Nature 150(3805):405–406. DOI: https://doi.org/10.1038%2F150405d0

Bai, T. (2003) Hot Spots for Solar Flares Persisting for Decades: Longitude Distributions of Flares of Cycles 19–23. Astrophys. J. 585:1114-1123. DOI: https://dx.doi.org/10.1086/346152

Bai T. and Cliver E. W. (1990) A 154 day periodicity in the occurrence rate of proton flares. Astrophys. J. 363:299–309. DOI: https://doi.org/10.1086/169342

Banerdt, W.B., Smrekar, S.E., Banfield, D. et al. (2020) Initial results from the InSight mission on Mars. Nat. Geosci. 13:183–189. DOI: https://doi.org/10.1038/s41561-020-0544-y

Bulow, R.C., Johnson, C.L., Bills, B.G., Shearer, P.M. (2007) Temporal and spatial properties of some deep moonquake clusters. J. Geophys. Res. 112:E09003. DOI: https://doi.org/10.1029/2006JE002847

Burrell, A.G., Sánchez-Cano, B., Witasse, O., Lester, M., Cartacci, M. (2020) Comparison of terrestrial and Martian TEC at dawn and dusk during solstices. Earth Planets Space 72:140 (2020). DOI: https://doi.org/10.1186/s40623-020-01258-3

Cane, H.V., Richardson, I.G., von Rosenvinge, T.T. (1998) Interplanetary magnetic field periodicity of ~153 days. Geophys. Res. Lett. 25(24):4437–4440. DOI: https://doi.org/10.1029/1998GL900208

Ceylan, S., Clinton, J.F., Giardini, D. et al. (2021a) Companion guide to the marsquake catalog from InSight, Sols 0–478: Data content and non-seismic events. Phys. Earth Planet. Inter. 310:106597. DOI: https://doi.org/10.1016/j.pepi.2020.106597

Ceylan, S., Clinton, J.F., Horleston, A., et al. (2021b) The Seismicity on Mars as Recorded by Insight's Marsquake Service. Presentation at the Annual Meeting of the Seismological Society of America, 23 Apr. https://seismosoc.secure-platform.com/a/solicitations/24/sessiongallery/380/application/6767, https://www.seismosoc.org/news/seismicity-on-mars-full-of-surprises-in-first-continuous-year-of-data-collection

Chowdhury, P., Kudela, K. Moon, Y.J. (2016) A Study of Heliospheric Modulation and Periodicities of Galactic Cosmic Rays During Cycle 24. Sol. Phys. 291:581–602. DOI: https://doi.org/10.1007/s11207-015-0832-7

Chowdhury, P., Khan, M., Ray, P.C. (2009) Intermediate-term periodicities in sunspot areas during solar cycles 22 and 23. Mon. Not. R. Astron. Soc. 392(1):1159–1180. DOI: https://doi.org/10.1111%2Fj.1365-2966.2008.14117.x

Chowdhury, P., Ray, P.C., Ray, S. (2008) Periodicity of ~155 days in solar electron fluence. Indian J. Phys. 82:95–104.

Clinton, J.F., Ceylan, S., van Driel, M., Giardini, D. et al., (2021) The Marsquake catalogue from InSight, sols 0–478. Phys. Earth Planet. Inter. 310:106595 (corrected Supplementary Table 2). DOI: https://doi.org/10.1016/j.pepi.2020.106595

Connerney, J.E.P., Acuna, M.H., Wasilewski, P.J., Kletetschka, G., Ness, N.F., Reme, H., Lin, R.P., Mitchell, D.L. (2001) The global magnetic field of Mars and implications for crustal evolution. Geophys. Res. Lett. 28(21):4015–4018. DOI: https://doi.org/10.1029/2001GL013619

Das, R., Meneses, C. (2021) Scaling relations for energy magnitudes. J. Geophys. 64(1):1–11. ARK: https://n2t.net/ark:/88439/x063005

Das, R., Sharma, M.L., Wason, H.R., Choudhury, D., Gonzalez, G. (2019) A seismic moment magnitude scale. Bull. Seismol. Soc. Am. 109(4):1542–1555. DOI: https://doi.org/10.1785/0120180338

Den Hartog, J. (1985) *Mechanical Vibrations* (4th ed.) Dover Publications. ISBN 9780486647852

Denskat, K.U., Beinroth, H.J., Neubauer, F.M. (1983) Interplanetary Magnetic Field Power Spectra With Frequencies from 2.4 X 10 to the-5th Hz to 470 Hz from HELIOS-Observations During Solar Minimum Conditions. J. Geophys. 54(1):60–67. ARK: https://n2t.net/ark:/88439/y063880

Dimitropoulou, M., Moussas, X., & Strintzi, D. (2008) Enhanced Rieger type periodicities' detection in X-ray solar flares and statistical validation of Rossby waves' existence. Proc. Int. Astron. Union 4(S257):159–163. DOI: https://doi.org/10.1017/S1743921309029226

van Driel, M., Ceylan, S., Clinton, J. F., Giardini, D., Horleston, A., Margerin, L., et al. (2021) High-frequency seismic events on Mars observed by InSight. J Geophys. Res. Planets 126:e2020JE006670. DOI: https://doi.org/10.1029/2020JE006670

Dziewonski, A.M., Chou, T.-A., Woodhouse, J.H. (1981) Determination of earthquake source parameters from waveform data for studies of global and regional seismicity. J. Geophys. Res. Solid Earth 86(B4):2825–2852. DOI: https://doi.org/10.1029/JB086iB04p02825

Ferrazzini, V., Aki, K. (1987) Slow waves trapped in a fluid-filled infinite crack: Implication for volcanic tremor. J. Geophys. Res. 92(B9):9215–9223. DOI: https://doi.org/10.1029/JB092iB09p09215

Forgacs-Dajka, E., Borkovits, T. (2007) Searching for mid-term variations in different aspects of solar activity – looking for probable common origins and studying temporal variations of magnetic polarities. Mon. Not. R. Astron. Soc. 374:282–291. DOI: https://doi.org/doi:10.1111/j.1365-2966.2006.11167.x

Frohlich, C., Nakamura, Y. (2009) The physical mechanisms of deep moonquakes and intermediate-depth earthquakes: How similar and how different? Phys. Earth Planet. Inter. 173(3–4):365–374. DOI: https://doi.org/10.1016/j.pepi.2009.02.004

Gupta, H.K. (Ed.) (2011) *Encyclopedia of Solid Earth Geophysics*. Springer. ISBN 9789048187010. DOI: https://doi.org/10.1007/978-90-481-8702-7

Gurgenashvili, E., Zaqarashvili, T.V., Kukhianidze, V., Oliver, R., Ballester, J.L., Dikpati, M., McIntosh, S.W. (2017) North–South Asymmetry in Rieger-type Periodicity during Solar Cycles 19–23. Astrophys. J. 845(2):137–148. DOI: https://dx.doi.org/10.3847/1538-4357/aa830a

Halekas, J.S., Poppe, A.R., Harada, Y., Bonnell, J.W., Ergun, R.E., McFadden, J.P. (2018) A tenuous lunar ionosphere in the geomagnetic tail. Geophys. Res. Lett. 45:9450–9459. DOI: https://doi.org/10.1029/2018GL079936

Harada, Y., Machida, S., Saito, Y., Yokota, S., Asamura, K. et al. (2010) Interaction between terrestrial plasma sheet electrons and the lunar surface: SELENE (Kaguya) observations, Geophys. Res. Lett. 37:L19202. DOI: https://doi.org/10.1029/2010GL044574

Jacoby, W.R. (2001) Successes and failures in geodynamics: from past to future. J. Geodyn. 32:3–27. DOI: https://doi.org/10.1016/S0264-3707(01)00026-6

Kanamori, H. (1977) The energy release in great earthquakes. J. Geophys. Res. Solid Earth Planets 82(29):2981–2987. DOI: https://doi.org/10.1029/JB082i020p02981

Kinkhabwala, A. (2013) Maximum Fidelity. Max Planck Institute of Molecular Physiology report. arXiv: https://doi.org/10.48550/arXiv.1301.5186

Knapmeyer, M., Stähler, S.C., Daubar, I., Forget, F., Spiga, A., et al. (2021) Seasonal seismic activity on Mars. Earth Planet. Sci. Lett. 576:117171. DOI: https://doi.org/10.1016/j.epsl.2021.117171

Kurochkin, N.E. (1998) Transient periodicity in solar activity. Astron. Astrophys. Trans. 15(1-4):277–279. DOI: https://doi.org/10.1080/10556799808201781

LaViolette, P.A. (1983) Galactic explosions, cosmic dust invasions, and climatic change. Ph.D. dissertation, Portland State University, pp.737. URI: https://search.library.pdx.edu/permalink/f/p82vj0/CP71128014660001451

Li, W., Raeder, J., Thomsen, M.F., Lavraud, B. (2008) Solar wind plasma entry into the magnetosphere under northward IMF conditions. J. Geophys. Res. 113:A04204. DOI: https://doi.org/10.1029/2007JA012604

Lorenz, R.D., Panning, M. (2018) Empirical recurrence rates for ground motion signals on planetary surfaces. Icarus 303:273–279. DOI: https://doi.org/10.1016/j.icarus.2017.10.008

Lorenz, R.D., Nakamura, Y., Murphy, J.R. (2017) Viking-2 seismometer measurements on Mars: PDS data archive and meteorological applications. Earth Space Sci. 4:681–688. DOI: https://doi.org/10.1002/2017EA000306

Nakamura, Y., Latham, G.V., Dorman, H.J., Harris, J.E. (1981) Passive Seismic Experiment, Long Period Event Catalog, Final Version. Institute for Geophysics, University of Texas at Austin. URI: https://hdl.handle.net/2152/65671

Odintsov, S., Boyarchuk, K., Georgieva, K., Kirov, B., Atanasov, D. (2006) Long-period trends in global seismic and geomagnetic activity and their relation to solar activity. Phys. Chem. Earth 31(1–3):88–93. DOI: https://doi.org/10.1016/j.pce.2005.03.004

Ogawa, M. (2007) Mantle convection: A review. Fluid Dyn. Res. 40(6):379–398. DOI: https://doi.org/10.1016/j.fluiddyn.2007.09.001

Omerbashich (2021a) Detection and mapping of Earth body resonances with cGPS. In press. DOI: https://doi.org/10.5281/zenodo.4678317

Omerbashich, M. (2020a) Earth body resonance. J. Geophys. 63:15-29. ARK: https://n2t.net/ark:/88439/x020219

Omerbashich, M. (2020b) Moon body resonance. J. Geophys. 63:30-42. ARK: https://n2t.net/ark:/88439/x034508

Omerbashich M. (2007a) Magnification of mantle resonance as a cause of tectonics. Geod. Acta. 20(6):369–383. DOI: https://doi.org/10.3166/ga.20.369-383

Omerbashich, M. (2007b) Erratum due to journal error. Comp. Sci. Eng. 9(4):5–6. DOI: https://doi.org/10.1109/MCSE.2007.79; full text: https://arxiv.org/abs/math-ph/0608014

Omerbashich, M. (2006a) Springtide-induced magnification of Earth mantle resonance causes tectonics and conceals universality of physics at all scales. arXiv. DOI: https://doi.org/10.48550/arXiv.physics/0608026

Omerbashich, M. (2006b) Gauss–Vaníček Spectral Analysis of the Sepkoski Compendium: No New Life Cycles. Comp. Sci. Eng. 8(4):26–30. DOI: https://doi.org/10.1109/MCSE.2006.68

Özgüç, A., Ataç, T. (1994) The 73-day periodicity of the flare index during the current solar cycle 22. Sol. Phys. 150:339–346. DOI: https://doi.org/10.1007/BF00712895

Pagiatakis, S. (1999) Stochastic significance of peaks in the least-squares spectrum. J. Geod. 73:67–78. DOI: https://doi.org/10.1007/s001900050220

Phillips, T. (2008) The Moon and the Magnetotail. NASA's Goddard Space Flight Center, NASA Space News, 16 Apr. http://web.archive.org/web/20210225013348/https://www.nasa.gov/topics/moonmars/features/magnetotail_080416.html

Press, W.H., Teukolsky, S.A., Vetterling, W.T., Flannery, B.P. (2007) *Numerical Recipes: The Art of Scientific Computing* (3rd Ed.). Cambridge University Press. ISBN 9780521880688

Ramstad, R., Brain, D.A., Dong, Y., Espley, J., Halekas, J., Jakosky, B. (2020) The global current systems of the Martian induced magnetosphere. Nat. Astron. 4:979–985. DOI: https://doi.org/10.1038/s41550-020-1099-y

Richter, F., McKenzie, D. (1977) Simple plate models of mantle convection. J. Geophys. 44(1):441-471. ARK: https://n2t.net/ark:/88439/y001916

Rieger, E., Share, G.H., Forrest, D.J., Kanbach, G., Reppin, C., Chupp, E.L. (1984) A 154-day periodicity in the occurrence of hard solar flares? Nature 312:623–625. DOI: https://doi.org/10.1038/312623a0

Russell, C.T. (2001) The dynamics of planetary magnetospheres. Planet. Space Sci. 49(10–11):1005–1030. DOI: https://doi.org/10.1016/S0032-0633(01)00017-4

Shang, W.S., Tang, B.B., Shi, Q.Q., Tian, A.M., Zhou, X.-Y., Yao, Z.H., et al. (2020) Unusual location of the geotail magnetopause near lunar orbit: A case study. J. Geophys. Res. Space Phys. 125:e2019JA027401. DOI: https://doi.org/10.1029/2019JA027401

Shannon, C.E. (1948) A Mathematical Theory of Communication. Bell System Tech. J. 27:379–423, 623–656. DOI: https://doi.org/10.1002/j.1538-7305.1948.tb01338.x

Simpson, J.F. (1968) Solar activity as a triggering mechanism for earthquakes. Earth Planet. Sci. Lett. 3:417–425. DOI: https://doi.org/10.1016/0012-821X(67)90071-4

Singh, Y.P., Badruddin (2019) Study of the solar rotational period and its harmonics in solar activity, interplanetary, geomagnetic, and cosmic ray intensity indicators during solar polarity reversal periods. Sol. Phys. 294:27. https://doi.org/10.1007/s11207-019-1413-y

Steeves, R.R. (1981). A statistical test for significance of peaks in the least squares spectrum. Collected Papers, Geodetic Survey, Department of Energy, Mines and Resources. Surveys and Mapping Branch, Ottawa Canada, pp. 149–166. URI: http://www2.unb.ca/gge/Research/GRL/LSSA/Literature/Steeves1981.pdf

Stevenson, D.J. (2008) A planetary perspective on the deep Earth. Nature 451:261-265. DOI: https://doi.org/10.1038/nature06582

Suemoto, Y., Ikeda, T., Tsuji, T. (2020) Temporal variation and frequency dependence of seismic ambient noise on Mars from polarization analysis. Geophys. Res. Lett. 47:e2020GL087123. DOI: https://doi.org/10.1029/2020GL087123

Taylor, J., Hamilton, S. (1972) Some tests of the Vaníček Method of spectral analysis. Astrophys. Space Sci. 17:357–367. DOI: https://doi.org/10.1007/BF00642907

Trotignon, J.G, Parrot, M., Cerisier, J.C., Menvielle, M., Axford, W.I., Paetzold, M., Warnant, R., Wernik, A.W. (2000) The plasma environment of Mars: from the shocked solar wind down to the ionosphere. Planet. Space Sci. 48(12–14):1181–1191. DOI: https://doi.org/10.1016/S0032-0633(00)00102-1

Tucker, O.J., Farrell, W.M., Poppe, A.R. (2021) On the effect of magnetospheric shielding on the lunar hydrogen cycle. J. Geophys. Res. Planets 126:e2020JE006552. DOI: https://doi.org/10.1029/2020JE006552

Vaníček, P. (1969) Approximate Spectral Analysis by Least-Squares Fit. Astrophys. Space Sci 4(4):387–391. DOI: https://doi.org/10.1007/BF00651344

Vaníček, P. (1971) Further Development and Properties of the Spectral Analysis by Least-Squares Fit. Astrophys. Space Sci. 12(1):10–33. DOI: https://doi.org/10.1007/BF00656134

Walsh, A.P., Haaland, S., Forsyth, C., Keesee A.M., Kissinger, J., Li, K., Runov, A., Soucek, J., Walsh, B.M., Wing, S., Taylor, M.G.G.T. (2014) Dawn–dusk asymmetries in the coupled solar wind–magnetosphere–ionosphere system: a review. Ann. Geophys. 32:705–737. DOI: https://doi.org/10.5194/angeo-32-705-2014

Wang, H.Z., Zhang, J., Shi, Q.Q., Saito, Y., Degeling, A.W., Rae, I.J., Zong, Q.G., Wei, Y., Liu, J., Guo, R.L. (2021) Earth Wind as a Possible Exogenous Source of Lunar Surface Hydration. Astrophys. J. Lett. 907(2):L32. DOI: https://doi.org/10.3847/2041-8213/abd559

Wells, D.E., Vaníček, P., Pagiatakis, S. (1985) Least squares spectral analysis revisited. Department of Geodesy & Geomatics Engineering Technical Report 84, University of New Brunswick, Canada. Link: http://www2.unb.ca/gge/Pubs/TR84.pdf

Yegorkin, A.V., Chernyshov, N.M. (1983) Peculiarities of Mantle Waves from Long-Range Profiles. J. Geophys. 54(1):30-34. ARK: https://n2t.net/ark:/88439/y090547